Classical Superconductors Materials, Structures and Properties

Michael R. Koblischka and Anjela Koblischka-Veneva

Abstract In this chapter, we discuss the structures and properties of classical (or conventional) superconductors, often dubbed also low-T_c materials (LTSc). Among them are elemental superconductors, being superconductors at ambient conditions or under pressure, and several metallic alloys. Among them are the systems NbTi, NbN, and Nb_3Sn, which are the so-called workhorses of superconductivity for nearly all types of applications, even today. Then, there are several families of materials with interesting outstanding superconducting and/or crystallographic properties like the heavy-fermion superconductors, the Chevrel phases, borocarbides, 2D materials or layered superconductors. For basic research questions, the metallic superconductors are ideal materials when preparing mesoscopic superconductor structures for the investigation of superconductivity in reduced dimensions. With the discovery of MgB_2 with a T_c of 38 K in 2001, the border to the high-T_c materials was crossed, thus triggering a lot of research efforts in the field. Besides this big push, the field of conventional superconductors is still progressing—new materials like the superconducting high entropy alloys (HEAs) and new families like the $LaBi_3$ superconductors or superconducting magic-angle graphene were discovered—stimulating the research in the field of superconductivity even further. Among the new experiments carried out are high-pressure experiments on the HEAs and even on NbTi, which was never done before. These experiments gave remarkable results showing NbTi being a superconductor with increased T_c ~ 19 K even up to 261 GPa. And finally, the high-pressure research on H_3S and LaH_{10} led to record, nearly room-temperature T_c's for materials belonging to the conventional superconductors.

Keywords Superconductors · Conventional superconductivity · Metals · Alloys · Chevrel phases · Heavy fermions · 2D superconductors · High entropy alloys · High pressure

M. R. Koblischka (✉) · A. Koblischka-Veneva
Experimental Physics, Saarland University, P.O. Box 151150, 66041 Saarbrücken, Germany
e-mail: m.koblischka@ieee.org; m.koblischka@gmail.com

A. Koblischka-Veneva
e-mail: a.koblischka@gmail.com

Y. Slimani and E. Hannachi (eds.), *Superconducting Materials*,
https://doi.org/10.1007/978-981-19-1211-5_6

1 Introduction

Superconductivity was discovered in Hg by H. Kamerlingh Onnes in 1911 [1, 2] by accident when trying to answer the question what the resistance will do at ultralow temperatures after having established the liquefaction of He. Mercury (Hg), being a liquid at ambient conditions, was the best choice to obtain very pure samples by multiple distillation. Hg was found to be a superconductor below $T_c = 4.15$ K, just below the temperature of liquid Helium (4.2 K). It took then some time to find other metallic elements showing the same superconducting transition, including the metals Sn and Pb with $T_c = 7.2$ K [3–8], being well above 4.2 K, followed by Nb with a T_c of 9.15 K, which is the highest one of all elements in ambient conditions. However, all these materials did not allow to produce a superconducting coil to generate magnetic fields without losses, which already Onnes had planned. The next step forward was NbN with a T_c of 16_K, followed by the alloys NbTi and V_3Si in the 1950s, which set the base for the development of real conductors with improved high-field properties [3, 7]. In this period, also fruitful empirical rules like the Matthias' rules were developed to enable the search for new superconductors, especially among the metallic alloys [9, 10]. The A15-alloys like Nb_3Sn, and the long-time T_c-record holder, Nb_3Ge with $T_c = 23.2$ K [11], were then developed in a quest to improve T_c further. Besides this, new families of superconductors were discovered from the 1960s onwards like the Chevrel phases [12], the heavy-fermion superconductors [13] and the borocarbides [14]. All the main development in this field then focused on the conductor development and some other applications like superconducting sensor elements, Josephson circuits including super-computers [4, 6]. Besides the big push with the upcoming of the high- T_c superconductors in 1986 [15], the field of conventional superconductivity did not die out, however, T_c could only be improved in 2001 [16] when MgB_2 was found to be a superconductor. As the conventional superconductors are metals, the samples could always be produced with high purity, making these systems most interesting for basic research questions. This opened up new fields like layered superconductors and mesoscopic superconductors, which are most interesting to investigate superconductivity in reduced dimensions like in nanowires or nanoparticles [17, 18]. Also, the search for new superconductors has never stopped, and so new systems like the ones with $AuCl_3$-structure [19] and the high-entropy alloys (HEAs) [20] were found. This quest for new superconductors is nowadays pushed forward by machine-learning search of databases [21–23]. Moreover, the recent high-pressure experiments on the HEAs [24], on NbTi [25], H_3S [26] and the La (super)hydrides (LaH_{10}) [27] brought out very interesting and remarkable results, with T_c reaching practically room-temperature. This further stimulated the research on the question if metallic hydrogen could be a superconductor [28, 29]. Thus, there are still many open questions to be answered, and so the field of conventional superconductivity remains to be very important.

2 Superconducting Elements

All superconductors marked green in Fig. 1 are metals, whereas also semimetals and non-metals can become superconductors under high pressure conditions (violet). There are some remarkable elements like carbon, which can be a superconductor with $T_c = 15$ K in form of carbon nanotubes [30], Boron-doped diamond films with $T_c = 4$ K [31], and recently as magic-angle bi-layered graphene with T_c ranging between 0.5 and 3 K [32–34]. Cr can be a superconducting material only as thin film [35], and Pd is a superconductor when being irradiated with He^+-ions [36]. Recently, also for Bi a T_c was obtained in ambient conditions, although very low ($T_c = 0.53$ mK, [37]) as compared to the several high-pressure phases of Bi, reaching 8.7 K (9 GPa). The same applies for Li, which was found to be superconductor at ambient conditions with $T_c = 4$ mK, but having $T_c = 20$ K at 50 GPa pressure [38]. Remarkable is further that even Fe may be a superconductor at $T_c = 2$ K under pressure [39]. Note also the very high T_c's for the non-metals B, O, S, P, and Se. Superconductivity for metallic hydrogen is still an open question ("??"), but with remarkable predictions to be a room-temperature superconductor [28, 29].

Nb is the element with the highest $T_c = 9.2$ K in ambient conditions, closely followed by the radioactive element, Tc, with $T_c = 7.8$ K [40]. Figure 2 presents T_c as a function of the year of discovery following Refs. [41, 42]. The blue symbols denote the elements superconducting at ambient conditions, and the red symbols such being superconducting only under pressure.

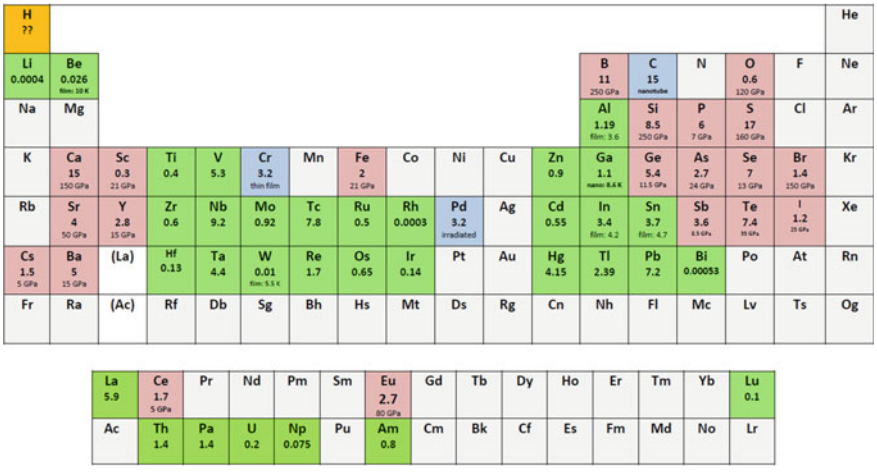

Fig. 1 Superconducting elements in the periodic table. The green color denotes elements being superconducting in ambient conditions, violet color denotes elements being superconductors under pressure. Light blue indicates elements being superconducting only under special conditions, see text. For some elements, a second T_c is given when in thin film or nanosized form. Hydrogen is marked orange with "??" for T_c, pointing to the big challenge for future investigations ("metallic H"). Drawn using data collected from Refs. [3–8, 30–43]

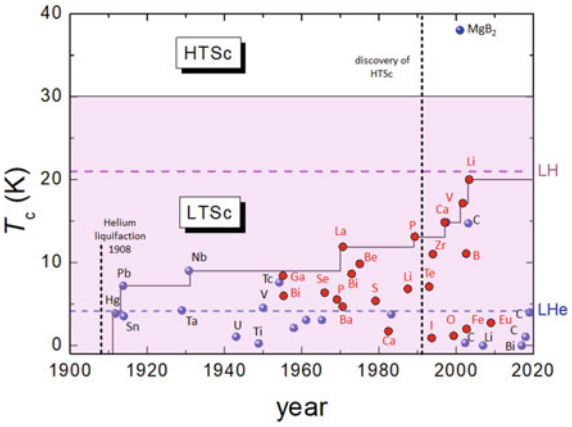

Fig. 2 T_c as a function of the year of discovery of the superconducting elements (blue—ambient conditions, red—under pressure). Note the highest T_c of all elements at 20 K for Li under pressure. Also presented are the borderlines for liquid He and liquid H. The 30 K-line marks the border between LTSc and HTSc materials, crossed by MgB_2, which is given for comparison

The bold line shows the upper T_c-limit as function of time. Table 1 gives a compilation of the superconducting properties (London penetration depth, λ_L, the coherence length, λ_L and the critical field, B_c, of some elemental superconductors, together with the respective crystal structure and the Debye temperature, Θ_D, which describes the lattice vibrations and the melting point. Note that all superconducting elements are type-1 superconductors (see chapter "Magnetic Properties of Superconducting Materials"), except Nb, which has a κ being very close to the borderline between type-1 and type-2 superconductors, so pure Nb is 'just' a type-2 superconductor. Table 2 presents the T_c-values of some of the elements being superconductors under pressure, including the latest element found to be a superconductor, Eu [43]. It is remarkable that the T_c-values obtained can be relatively high as compared to the elements at ambient conditions, and are exceptionally high for Li (20 K at 50 GPa, but 0.4 mK ambient), which holds the T_c-record of all elements, followed closely by P (18 K). Buzea and Robbie have reviewed the so-called puzzle of superconducting elements, as it is not straightforward to determine a clear rule if a material will be a superconductor or not [41]. The data presented in Tables 1 and 2 clearly reveal further that there is no simple relation between T_c and the respective crystal structure or the Debye temperature, Θ_D, but as described in Refs. [44, 45], a relation between a characteristic crystallographic length, x, and T_c does exist which enables a simple calculation of T_c with the only knowledge of the electronic structure and the crystallographic data [46, 47]. This approach, called Roeser-Huber formula, can directly be proven using superconducting elements being superconducting with more than one crystal structure, also called polymorphs (Fig. 3).

Such cases can indeed be found for Hg (see Table 1), and especially, for La with the two structures *fcc* ($T_c = 6$ K) and *dhcp* (double hexagonal close-packed, with $T_c = 4.8$ K) [41]. The application of the Roeser-Huber formula and the search principles for the characteristic length x in the crystal structure brings out the correct values for the respective T_c values.

Table 1 T_c of some superconducting elements in alphabetical order, together with their crystal lattice, melting point and some superconducting properties. Data were collected from Refs. [3, 30–43]. The crystal structures are *fcc*—face-centered cubic, *bcc*—body-centered cubic, *hex.* —hexagonal, *dhcp*—double hexagonal close packed, *rhomb.*—rhombohedral, *tetr.*—tetragonal and *orth.*—orthorhombic

Element	T_c (K)	Crystal structure	Melting point (°C)	Θ_D (K)	λ_L (nm)	ξ_{GL} (nm)	B_c (mT)
Al	1.18	*fcc*	660	420	50	1600	10
Bi	0.00053	*trigonal*	271.4	112	0.16	96,000	0.0052
Cd	0.52	*hex*	321	300	130	760	3
Ga	1.08	*orth*	29.8	317	120		5.9
Hg	4.15 3.95	*rhomb* *tetr*	−38.9 –	90 –	– –	55 –	40 34
In	3.4	*tetr*	156	109	24–64	360–440	28
La	5.9 4.8	*fcc* *dhcp*	– –	– –	– –	– –	– –
Nb	9.2	*fcc*	2500	240	32–44	39–40	195
Pb	7.2	*fcc*	327	96	32–39	51–83	80
Re	1.7	*hex*	3180	430	–	–	19
Ru	0.5	*hex*	2500	600	–	–	6.6
Sn	3.7	*tetr*	231.9	195	25–50	120–320	30.5
Ta	4.4	*bcc*	3000	260	35	93	80
Th	1.4	*fcc*	1695	170			15
V	5.4	*bcc*	1730	340	39.8	45	120
W	0.01	*bcc*	3380	390	–	–	0.124
Zn	0.85	*hex*	419	310		25–32	5.2

Table 2 T_c of elements being superconducting only under pressure. Data were collected from Refs. [3, 30–43]

Element	T_c (K)	Pressure (MPa)
As	2.7	24
Ba	5.1	20
Bi-II Bi-III Bi-V	3.9 7.2 8.7	2.6 >2.7 >9
Eu	2.7	142
Fe	2	21
Ge	5.4	11.5
Li	20	50
P	18	30
Se	6.9	13
Si	8.5	12
Te	7.4	35

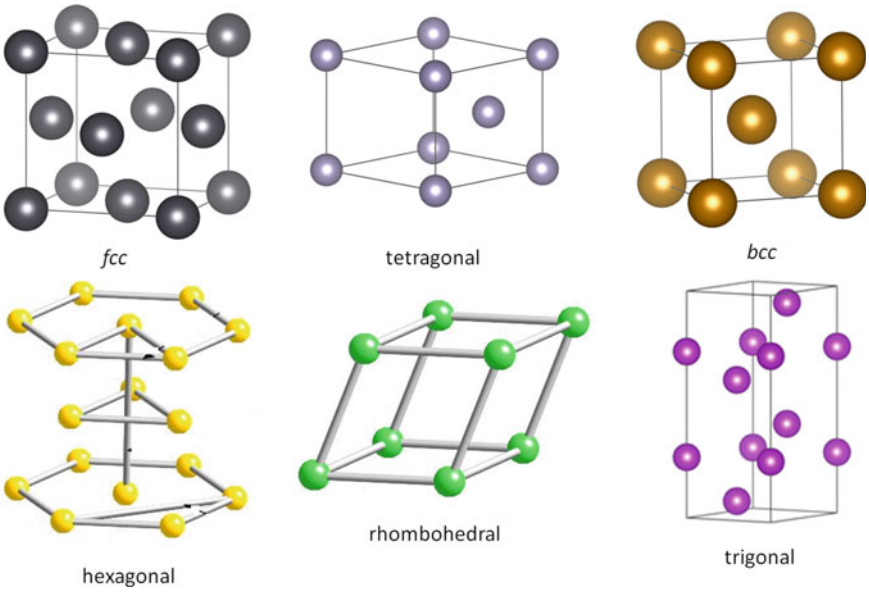

Fig. 3 Typical crystal structures of the superconducting elements (see also Table 1). Crystal structures were drawn using VESTA software [48] and the data files were performed based on X-ray databases [49–51]

The puzzle of the superconducting elements gets an additional complication when preparing superconductors in reduced dimensions (e.g., as nanostructured thin films (2D/1D), as nanowires (1D) or nanowire arrays or even nanoparticles (0D)). In thin film form, which acts as a platform for geometrically confined, strongly interacting electrons, several superconductors exhibit higher T_c's (the most famous example are here Al thin films with T_c raising from 1.2 K up to 4 K [52]), and other materials follow the more common understanding showing their T_c being reduced with decreasing the film thickness. All such experiments were summarized by Ivry et al. [53], which certainly contributes to gain better understanding of these effects.

Another complication is offered when approaching 1D or 0D dimensions with nanowires and nanoparticles prepared from superconducting materials. Several observations of unexpected phenomena were reported in the literature, e.g., Pb films with thickness-dependent oscillating behavior of T_c [54], and Al-nanowires exhibiting size-dependent breakdowns of superconductivity [55].

A recent example should be mentioned here in more detail: Samples of nanostructured β-Ga wires were recently prepared by a novel method of metallic-flux nanonucleation in alumina templates [56] allowing the determination of several superconducting parameters via magnetic measurements. The Ga nanowires could be described as a weak-coupling type-2 superconductor with $\kappa = 1.18$, favorized by the nanoscopic scale of the Ga nanowires. This result and the relatively high T_c

of 6.2 K reported is in stark contrast to pure bulk Ga, which is a type-I superconductor with $T_c \sim 1.1$ K [57, 58]. The fabrication techniques of such 1D-nanowires were recently reviewed by Koblischka and Koblischka-Veneva [59], and similar effects were observed also in other superconducting materials when being prepared in nanowire form. The topic of superconductivity in reduced dimensions and the possible increase of T_c will certainly deliver new surprises in the future.

A set of empirical rules was established in 1957 by Matthias [9, 10], which is commonly referred to as Matthias' rule. Although there is no apparent regularity in the occurrence of super-conductivity and the placement of the element in the periodic table, the rules provide certain useful traits for the search of new superconducting materials. The main idea is to qualitatively relate the superconducting transition temperature, T_c, to the valence electrons per atom, *e*/a. When looking at this relation for non-transition elements (e.g., closed *d*-shell), T_c is a smooth increasing function of the *e*/a, while for the transition metals, when being in stable crystalline form, the resulting function shows peaks in T_c for *e*/a values of 3, 5, and 7. This function is shown in Fig. 4, indicating the transition period and the period of closed *d*-shell. Another rule concerns the crystal symmetry, saying 'high symmetry is good, cubic symmetry is the best'. Other rules contain recommendations like 'Stay away from magnetism', which is a quite understandable advice, or 'Stay away from oxygen and insulators', but many new unconventional superconductors have broken these rules. For most metals, and especially for the main superconducting alloys and intermetallic compounds, the rules have worked fairly well, helping researchers a lot to find new superconducting materials.

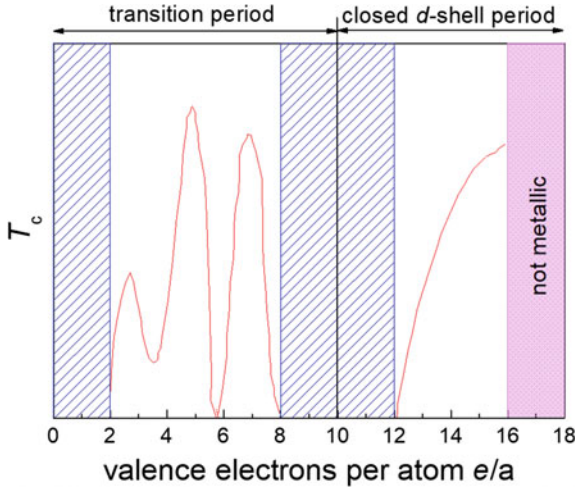

Fig. 4 Matthias' rule, showing T_c as function of the valence electron count, *e*/a. 3 peaks appear in the transition period, whereas a smooth curve is obtained in the closed *d*-shell period

3 Metallic Alloys and Intermetallic Compounds

The metallic alloys and intermetallic compounds are the largest group of all superconducting materials with more than 1000 members, reflecting the numerous combinations of metallic elements possible. In this chapter, we will therefore only focus on the five alloys and intermetallic compounds, which are the most important ones for applications, that is, NbN, NbTi, the A15-compounds with the most prominent member, Nb_3Sn, the Chevrel phases plus the newest member with the highest T_c of all metal alloys, the MgB_2 compound. Especially when considering superconductivity in the metallic alloys, the Matthias' rule proved its usefulness to find new superconducting materials.

3.1 NbN

The NbN material was the first binary compound with a T_c above 10 K discovered by Aschermann [60] in 1941. The optimum T_c is obtained to be 16 K, being much higher than that of the superconducting elements. NbN has a crystal structure of the rock-salt type (B1), and the lattice parameter and the achievable T_c depend strongly on the N content [61–63]. The material is attractive for applications especially in form of thin films [4, 64] for use in radio frequency cavities or as active element in single-photon detectors [65, 66]. NbN is typically sputtered (reactive DC magnetron sputtering) from Nb targets in controlled N_2-atmosphere on Si/SiO_2-substrates, and the heating of the substrate material is an important issue for the performance as it influences directly the sample resistance and the upper critical fields. As thin film material, nanostructuring with modern technologies like e-beam lithography or focused ion-beam milling is an important issue for further development.

3.2 NbTi

The alloy NbTi is the classical workhorse of superconductivity. Since its discovery in 1960, this material proved that it can be easily produced in wire form, even as multifilaments. The superconducting parameters including a T_c of approximately 10 K and an upper critical field of $B_{c2}(0) \sim 11.5$ T made it the material of choice for MRI applications and most laboratory equipment [67–69]. The Ti content in commercial NbTi conductors varies between 30 and 49%, and additions of, e.g., 20% Zr (for Ti) further strengthen the high field properties. The NbTi material has a *bcc* structure [70], which corresponds to that of Nb, whereas Ti has a hexagonal, close packed (*hcp*) crystal structure (P63/mmc). The size difference of Nb and Ti is only 2%, so the resulting lattice parameter, a, of NbTi is 0.3285 nm, slightly smaller than that of pure Nb. The component Ti itself is not superconducting down to 0.39 K at ambient

pressure [71]. Thus, the superconductivity depends mainly on the Nb component, and the bcc crystal structure must be maintained to keep up the T_c, which defines the limits of Ti and Zr additions. The effects of the metallurgical treatments and details of the composition on the flux pinning properties were discussed by Hillmann [72]. The development of NbTi wires for magnet applications is still ongoing [67], and also thin films of NbTi are of interest in the development of superconducting joints for HTSc conductors [73].

Very recently, high-pressure resistance measurements were performed as function of temperature and applied magnetic field on commercial NbTi alloy samples with the nominal composition $Nb_{0.44}Ti_{0.56}$, showing a T_c at ambient conditions of 9.6 K. Interestingly enough, such experiments were not carried out in all the years before. The interest in such experiments was now sparked by similar experiments carried out on the superconducting high-entropy alloys (HEA), which are based on the NbTi system. The properties of the HEA superconductors will be discussed in Sect. 2 below.

The high-pressure experiments on NbTi conducted in a non-magnetic diamond anvil cell by Guo et al. [25] showed an extraordinary robustness of superconductivity against pressure up to the very high pressure of 261 GPa. As illustrated in Fig. 5, this pressure corresponds to the outer core of Earth. The high-pressure experiments made NbTi now holding the record T_c and the record upper critical field, B_{c2}, for an alloy composed solely from transition elements. The high-pressure measurements also included XRD analysis, so Fig. 6 presents T_c as a function of the volume change $(-\Delta V/V_0)$ of the unit cell caused by the applied pressure. Both NbTi and the HEA alloy $(Tb, Nb)_{0.67}(Hf, Zr, Ti)_{0.33}$ with the same crystal structure (*bcc*) show a similar behavior, although with clearly different magnitude, as compared to the pure element Nb. The remarkable findings presented in [25] thus not only reveal the extraordinary high-pressure superconducting properties of a commercially fabricated NbTi alloy, but also give a new push forward to a better understanding of the mechanism of superconductivity in general.

3.3 A15-Compounds

The other big group of superconducting alloys important for applications are the so-called A15 superconductors. The A15-type superconductors (V_3Si and Nb_3Sn) were found by Hardy and Hulm [74] and Matthias [10, 75] in 1954. The history of these materials, which were since then the materials with the highest T_c known until the HTSc era, was recently reviewed by Stewart [76]. There are 69 distinct members of A15 compounds, from which 53 are superconductors, and 15 of them show a superconducting transition temperature of 10 K or higher. All the superconductors with the A15 structure are extreme type-2 superconductors and thus very important for the generation of large magnetic fields.

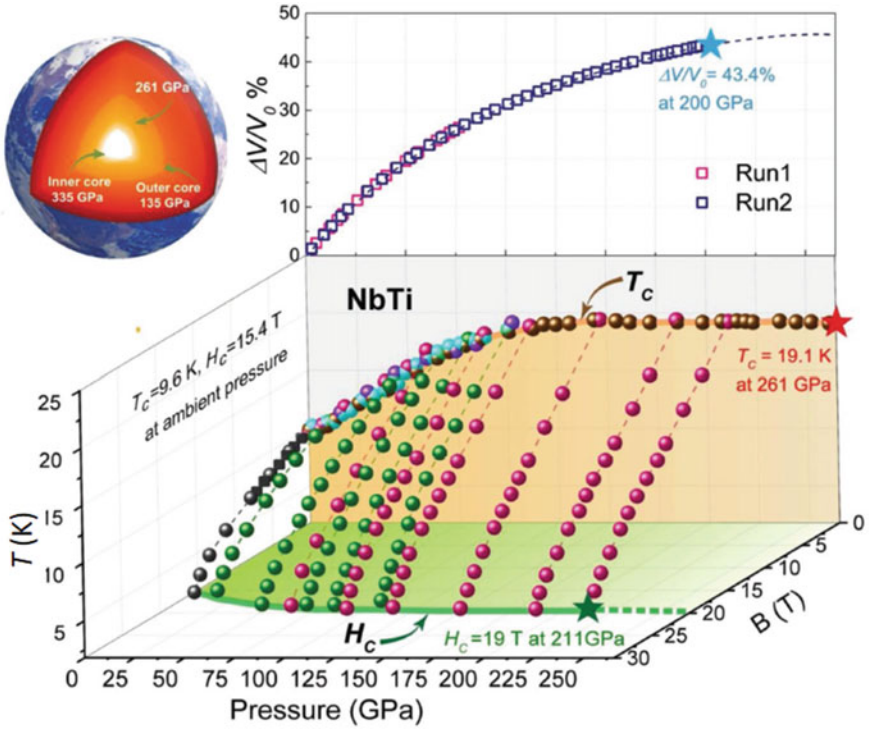

Fig. 5 High-pressure resistance measurements as function of applied magnetic field and temperature on NbTi. Data are taken in different experimental runs as indicated by the colors used. The red star marks the record T_c of 19.1 K at 261 GPa, the green one the highest critical field, B_{c2}, recorded at 19 T. The inset presents the pressures around Earth's core for comparison. Reproduced with permission from Ref. [25]

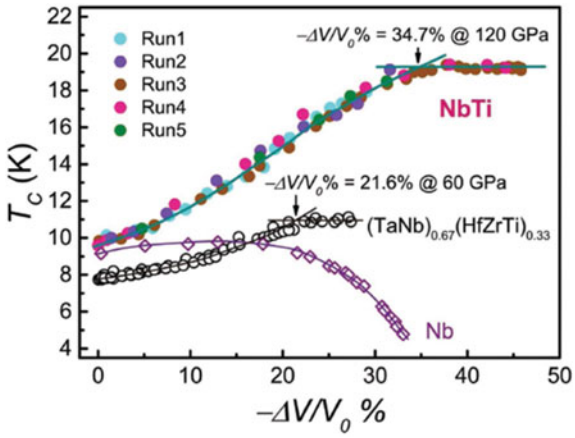

Fig. 6 High-pressure expeiment showing T_c as function of the volume change for NbTi, the HEA alloy $(Ta,Nb)_{0.67}(Hf,Zr,Ti)_{0.33}$ and that of elemental Nb for comparison. Reproduced with permission from Ref. [25]

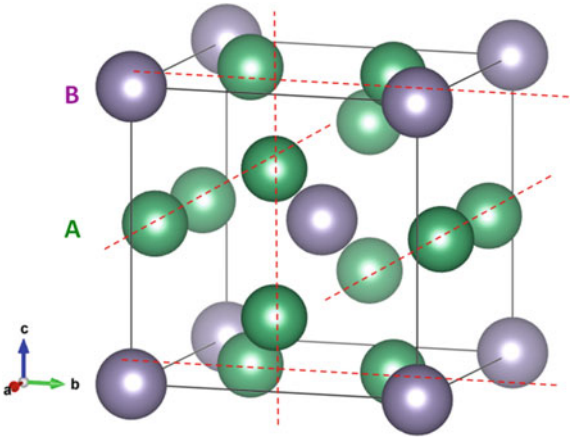

Fig. 7 Crystal structure of the A15-compounds. The dashed red lines indicate the chain directions, formed by the A-elements

The crystal structure of the A15 compounds is the β-tungsten structure. The prototype material of the A15-class is Cr_3Si (or abbreviated A_3B). The B-component occupies a *bcc* lattice, and on each crystal face, there are two atoms of the A-component. The crystal structure is depicted in Fig. 7. The lattice parameters are $a = b = c$ and $\alpha = \beta = \gamma = 90\circ$.

The superconducting transition temperatures were steadily increased from 18 K (Nb_3Sn, 1954) [74, 75], to 20 K ($Nb_3Al_{0.2}Ge_{0.8}$, 1967) [76], 20.3 K (Nb_3Ga, 1971) [77] and, finally, Nb_3Ge with a T_c of 22.3 K (1973) and further optimized in thin film form to the record value of 23.2 K in 1974 [78, 79]. The biggest problem is that the fabrication of wires from the A15 superconductors is a very complicated procedure as Nb_3Sn is a brittle intermetallic compound [4], but with a well-defined stoichiometry. The wire form is typically prepared by long term reactive diffusion, using Nb and Sn rods as the starting materials. To further improve the fabrication process and to prepare the required multifilamentary wires, several routes have been developed in the literature like the bronze route, the internal tin and the powder-in-tube technique [4, 5]. The production of the A15 conductors is mainly driven by the large projects on particle accelerators and fusion reactors, demanding high magnetic fields [80]. Therefore, many new developments are reported in this field still today, and the achieved progress concerning the critical current density is remarkable [81–83].

Another direction of research is the preparation of thin films of the A15 materials to be used in superconducting cavities. It is remarkable that the highest T_c of all A15 compounds was reached in the thin film state, where the substrate contributes to stabilizing the metastable Nb_3Ge compound. Also, in this branch of research, the work is still ongoing to further optimize the microstructures and the resulting superconducting properties [84].

3.4 Chevrel Phases

The intermetallic compounds known as Chevrel phases are ternary molybdenum chalcogenides, with the general formula $M_yMo_6X_8$, where M is a metal ion and X a chalcogen (S, Se, or Te). The Chevrel phases form a very interesting family of materials, and their unusual crystal structures were discovered by Chevrel et al. in 1971 [13, 85]. The superconductivity of these materials, with T_c values ranging up to 15 K, was first reported by Matthias et al. in 1972 [86]. In the following years, it was found that many members of this Chevrel phase family exhibited exceptionally high upper critical fields, which were clearly higher than the 20–40 T range of the A-15 superconductors [87, 88]. This observation made the Chevrel phase superconductors very unique, and very interesting for possible high-field applications [89]. In general, superconductivity is observed for compounds containing M = Li, Na, Sc, Pb, Sn, Cu, Ag, Zn, Cd, and almost all lanthanides, except Ce, Pm, and Eu [7]. Among the ternary compounds, the material $PbMo_6S_8$ (abbreviated as PMS) shows the highest T_c of 15 K and the upper critical field at $T = 4.2$ K reaches 60 T [4, 90, 91]. Thus, PMS is a material for high-field applications at low temperatures with an upper critical field clearly above that of Nb_3Sn.

The characteristic of all Chevrel-phase compounds with the chemical formula $M_yMo_6X_8$ contain Mo_6X_8 octahedra as basic building blocks of the rhombohedral-hexagonal structure with space group R(−3) as presented in Fig. 8. Each unit has in the form of a distorted cube or pseudo-cube with the X-atoms being located at the corners. The six Mo atoms are placed near the centers of each of its six faces, thus forming a dense cluster with the shape of a distorted Mo octahedron.

Looking at the various compositions possible, the intra-cluster distance varies from 0.267 nm for $Cu_{3.6}Mo_6S_8$ to 0.276 nm for Mo_6S_8 and the inter-cluster distance ranges from 0.308 nm for Mo_6S_8 to 0.366 nm for $PbMo_6Se_8$. The Mo-3d-orbitals are sufficiently extended allowing strong metallic bonding. The pseudo-cubes are stacked in an almost-cubic unit cell, with each of its one-eighth unit cells being occupied

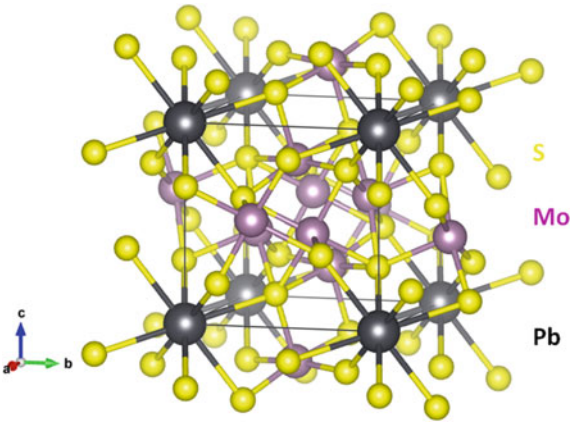

Fig. 8 Crystal structure of Chevrel phase compound $PbMo_6S_8$ (PMS)

by a Mo_6X_8 cluster. The side length of the unit cell is typically about 0.65 nm, and the extension of the embedded Mo_6S_8 cluster is about 0.38 nm. Both the intra- and inter-cluster distances were found in the literature to be important in controlling the T_c of the compound.

The superconducting parameters of the Chevrel phase compounds are quite special (see Fig. 9 and Table 3), placing these materials between the conventional metal systems and the HTSc materials. The anisotropy is >2, whereas the coherence length is ~2.5 nm, which is smaller than that of Nb_3Sn (3 nm), but larger as for the HTSc. Superconductivity in Chevrel-phase compounds was previously thought to be of conventional singlet *s*-wave type, although experimental data exhibit features of both conventional and unconventional superconductivity. Interestingly, recent studies have found them to be *d*-wave superconductors, and even multiband superconductivity has been manifested in PMS and SMS compounds in STS studies [7]. A full understanding of these unusual materials is still not reached yet. Nevertheless, Chevrel-phase superconductors are potential materials for ultrahigh-field applications due to their extremely high critical fields [4].

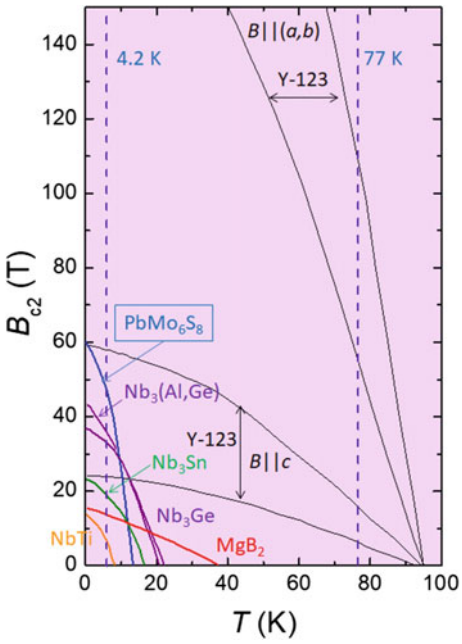

Fig. 9 Comparison of the upper critical fields, $B_{c2}(T)$, of $PbMo_6S_8$ (PMS) with $Nb_3(Al, Ge)$, Nb_3Ge, Nb_3Sn, NbTi, MgB_2 and the HTSc material Y-123 in the field directions $B \| c$ and $B \| (a, b)$. Data were collected from Ref. [91]

Table 3 Superconducting parameters of various Chevrel phase compounds. Data were collected from Refs. [3, 7]

Material	T_c (K)	B_{c2} (T)	λ_L (nm)	ξ_{GL} (nm)
$PbMo_6S_8$	15	60	240	2.3
$SnMo_6S_8$	12	34	240	3.5
$LaMo_6S_8$	7	45	–	3.1
$TbMo_6S_8$	1.65	0.2	–	45
$PbMo_6Se_8$	3.6	3.8	–	11
$LaMo_6Se_8$	11	5	–	9

3.5 *Magnesium Diboride, MgB_2*

Superconductivity in the MgB_2 system was found by Nagamatsu et al. in 2001 [16], showing a T_c of 38 K. This finding nearly doubled the previous record for the highest T_c of a metallic compound, crossing into the HTSc regime above 30 K. The material itself was not new, but never tested for superconductivity before. A reason for this may be the fact that neither element Mg nor B is superconducting itself, and both constituents are light metals without d-electrons, which were thought to be necessary for superconductors.

The crystal structure of MgB_2 is hexagonal of the type AlB_2 (space group C32, P6/mmm). The magnesium and boron atoms are arranged in sequent layers (see Fig. 10). The lattice parameters are $a = 0.3047$ nm and $c = 0.3421$ nm. The shortest distance between atoms is the B-B-spacing within the B-layer with $d = 0.176$ nm [92, 93].

The MgB_2 compound shows several remarkable properties including extreme type-2 superconductivity with high critical fields up to 14 T (bulks) and 74 T for thin films [7]. MgB_2 is the first established example of a multiband superconductor, possessing two distinct energy gaps of about 2 and 7 meV [94]. Owing to the close relation to the metallic superconductors, polycrystalline samples of MgB_2 were quickly found to show transparency of transport currents to the grain boundaries,

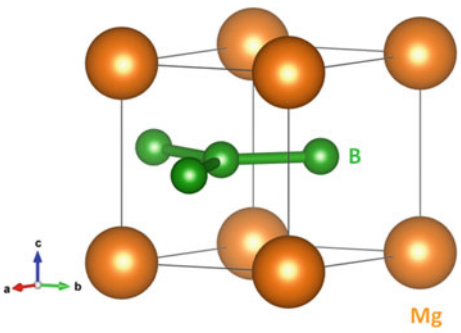

Fig. 10 Crystal structure of the MgB_2-compound showing the two different structures of Mg and the boron layer

which implies that the grain boundaries are not acting as weak links to degrade the critical currents as is the case for the cuprate HTSc superconductors [95, 96]. This observation sparked the interest in applications of MgB_2, as a much cheaper production route could lead to wires and bulk samples, even though the T_c is clearly below 77 K.

The MgB_2 crystal lattice shows two different atomic bindings, the covalent ones which are mostly typical for semiconductors and also metallic binding, being typical for conductive materials. These covalent bindings are strong, whereas the coupling between B and Mg between the layers is formed by metallic 3D π-bindings, which provide a weak coupling only [93]. Furthermore, the bindings within the Mg-plane are much stronger than the Mg-B-bindings [92]; thus, cleaving of the crystal can take place at this position [94]. The electronic structure of MgB_2 shows 4 bands crossing the Fermi niveau [97, 98]. Two π-bands, which result from the p_z-orbitals of the B-atoms and are weakly coupled with the phonon-modes (3D character). The two σ-bands result from the $p_{x,y}$-orbitals of the B-atoms. These are weakly coupled to the phonon-modes exhibiting 2D character [97, 99, 100]. Furthermore, there have been recently speculations that MgB_2 could belong to a new type of superconductivity, the type-1.5 superconductivity (see also chapter "Magnetic Properties of Superconducting Materials"), exhibiting similarities between type-1 and type-2 superconductivity, based on observations of the flux-line lattice [101]. This is a direct consequence of the multiband character of superconductivity in MgB_2. The MgB_2 compound is now considered as a strong competitor to the other metallic superconductors NbTi and Nb_3Sn, but offers also the possibility to operate at more elevated temperatures like 20_K, which can be cost-effectively generated by modern cryo-cooling systems. The fact that both ingredients abundantly available, and no expensive rare earth materials are involved, makes MgB_2 a cost-effective superconducting material, which can also compete with the HTSc for some applications. Thus, the development of fabrication processes of MgB_2 wires is strongly pushed forward [102], also benefitting from the lessons learned in the HTSc wire development.

4 Critical Currents and Fields, Conductor Development

4.1 Comparison of Critical Currents and Fields of Different Materials

The starting point for choosing an appropriate material for a given application is, of course, a proper choice of the superconducting properties of the respective material. Thus, it is very informative to have a look at the $j_c(T, B)$-diagram and compare the common wire materials NbTi, Nb_3Sn and the new MgB_2 with each other. Such a comparison of the $j_c(B, T)$-surfaces of MgB_2, NbTi and Nb_3Sn is depicted in Fig. 11. Nb_3Sn reveals the best high-field properties among these materials, but MgB_2 competes mostly well with NbTi—with the critical field being a bit low—but

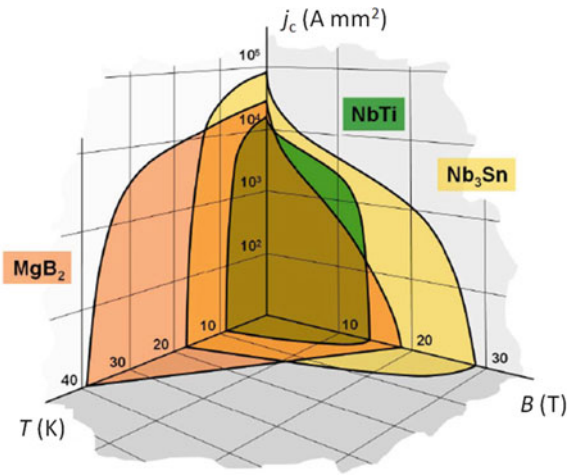

Fig. 11 Comparison of the 3D-surfaces $j_c(B,T)$ for the compounds MgB_2, NbTi and Nb_3Sn, following Ref. [103]

has the advantage of a possible operation at 20 K due to the much higher T_c. The data for the critical current density, j_c, at 4.2 K, the upper critical fields, B_{c2} at 4.2 K, the irreversibility fields, B_{irr} at 4.2 K and the superconducting parameters $\lambda(0)$ and $\xi(0)$ are given in Table 3 together with the electrical resistivity obtained at T_c.

Table 4 reveals that the critical fields of the HTSc compounds at 4.2 K are unbeatably high, whereas the size of the critical currents is comparable of all materials. The metallic alloys have the advantage of having no anisotropy effects, which makes them the best choice for applications at low temperatures and in their respective field range. It is also obvious from the data that MgB_2 belongs to the metallic alloys, showing a small anisotropy. However, the critical fields of MgB_2 at 4.2 K are relatively low, but when considering applications operating at 20 K, MgB_2 has a unique position among all superconducting materials.

Table 4 Comparison of the superconducting properties of NbTi, Nb_3Sn and MgB_2 with those of the HTSc compounds $YBa_2Cu_3O_x$ (YBCO) and $Bi_2Sr_2Ca_2Cu_3O_{10}$ (Bi-2223) (see also chapter "Noncuprate Superconductors: Materials, Structures and Properties")

Parameter	NbTi	Nb_3Sn	MgB_2	YBCO	Bi-2223
T_c (K)	9	18	39	92	110
anisotropy	Negligible	Negligible	1.5–5	5–7	50–200
j_c at 4.2 K (A/cm^2)	~10^6	~10^6	~10^6	~10^6	~10^7
B_{c2} (T) at 4.2 K	11–12	25–29	15–20	>100	>100
B_{irr} (T) at 4.2 K	10–11	21–24	6–12	5–7 (77 K)	0.2 (77 K)
$\xi(0)$ (nm)	4–5	3	4–5	1.5	1.5
$\lambda(0)$ (nm)	240	65	100 ~ 140	150	150
Resistivity $\rho(T_c)$ ($\mu\Omega$ cm)	60	5	0.4	150–800	40–60

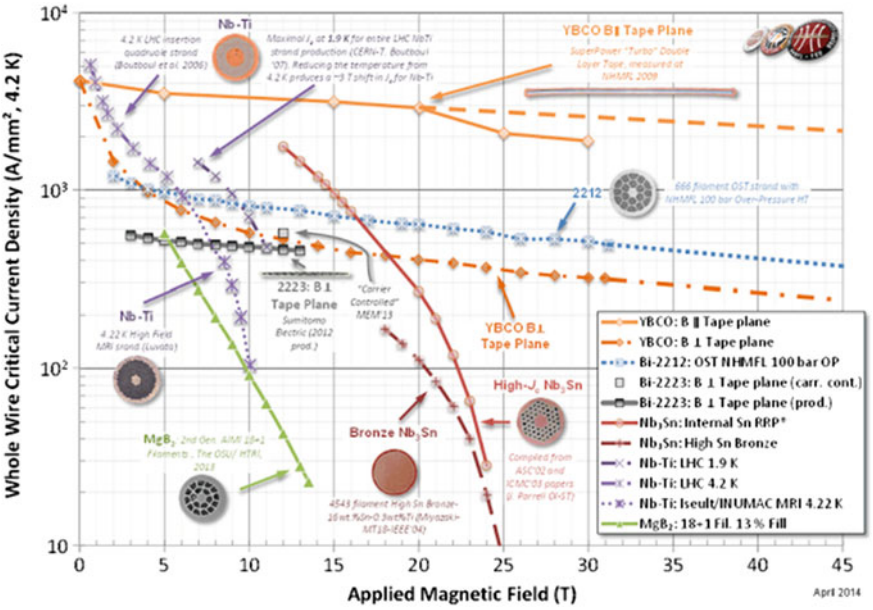

Fig. 12 Results of the critical current density (whole wire, $T = 4.2$ K) from various types of wire samples, including MgB_2-wires, NbTi, Nb_3Sn and the HTSc-compounds Bi-2212, Bi-2223 and YBCO [104]

Figure 12 presents data of the whole wire critical current density at $T = 4.2$ K (liquid Helium temperature) as function of the applied magnetic field. At the given low temperature, the HTSc materials show their ultimately high critical fields, but the critical currents of the nowadays well-developed Nb_3Sn and NbTi-wires can surpass the ones of the HTSc in an appropriate field range.

The critical current data of the MgB_2-wire are still the lowest ones, but of course, the MgB_2-wire production is still not as mature as that of NbTi, so there is hope for future developments improving the flux pinning properties.

4.2 Fabrication of Wires for Applications

Careful design is required to develop superconducting wires and cables as detailed in the reviews of wire manufacturing in Refs. [4, 5]. For different types of applications, the wire design needs to be adapted accordingly, which adds complexity to the wire architecture in the sense that also the outer shell and the manufacturing route have to be selected carefully to achieve the demanded superconducting properties.

NbTi is practically an ideal material for conductor fabrication, with no anisotropy (cubic crystal structure), the only metallic superconductor being ductile and being composed of only two constituents [5]. Figure 13 presents cross-section views of

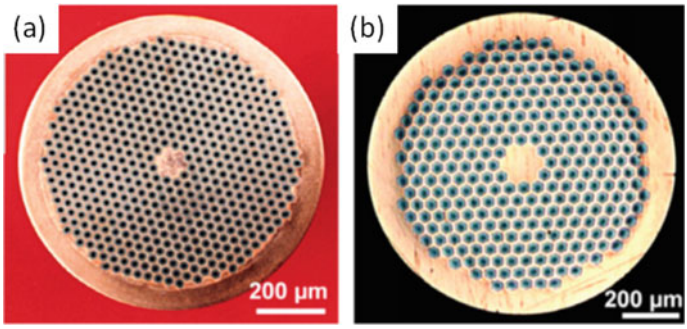

Fig. 13 Modern 504 filament (left) and 288 filament (right) PIT wires, manufactured by Shape Metal Innovations (SMI, Enschede, The Netherlands). Reproduced with permission from Ref. [105]

(a) a 504 filament and (b) 288 filament powder-in-tube (PIT) NbTi wires fabricated by Shape Metal Innovations (SMI). The properties of these wires were discussed in detail in Ref. [105]. However, as shown before in Fig. 12, the applicable field range for NbTi is limited up to 9 T, so for the high-field applications in laboratory magnets and the large particle colliders, Nb_3Sn wires are required for the magnet design [106]. In Ref. [107], the properties of Nb_3Sn wires for applications at CERN (Large Hadron Collider, LH-LHC quadrupoles) were discussed and the wires stemming from different manufacturers were compared to each other. This illustrated in Fig. 14a, b. Figure 14c, d present Nb_3Sn wires with different manufacturing processes from SMI (reinforced ternary PIT wire) and a wire fabricated by the ternary bronze route from Vacuumschmelze, respectively. A comprehensive discussion of the Nb_3Sn wire fabrication was presented by Godeke [108].

Accelerator magnets use high-current, multi-strand superconducting cables to reduce the number of turns in the coils, and thus magnet inductance [106]. A face view and the cross-sections of such a 40-strand Nb_3Sn cable are presented in Fig. 15.

Figure 16 presents the steps made towards an MgB_2-wire fabrication, which can profit from the existing knowledge of the other metallic compounds, but also from the lessons learned from the HTSc wires of the first generation. The images of Fig. 16 present a MgB_2 monofilament, the strand architecture, shaped wires and 3×3 and 12-strand cables. Even though the MgB_2 material is relatively new as compared to the metal alloys of the 1960_s, multifilament wires and cables of MgB_2 can already be manufactured, but there are still lot of efforts required to bring the MgB_2 wires to a similar stage like the metal alloys NbTi and Nb_3Sn. The current status of European MgB_2-wire manufacturing was recently reviewed in [105].

Finally, Fig. 17 illustrates the conductor development of the Chevrel phase superconductor, TMC (ternary Mo chalcogenides, i.e., the compound $PbMo_6S_8$). The superconducting material is packed in a Mo shell, and then into a stainless-steel tube to improve the mechanical properties as the final conductor is foreseen for high-field experiments [110, 111]. The extrusion billet shown weighs 1.5 kg. The TMC wires are not only working at much higher fields as those of Nb_3Sn, but may also have an

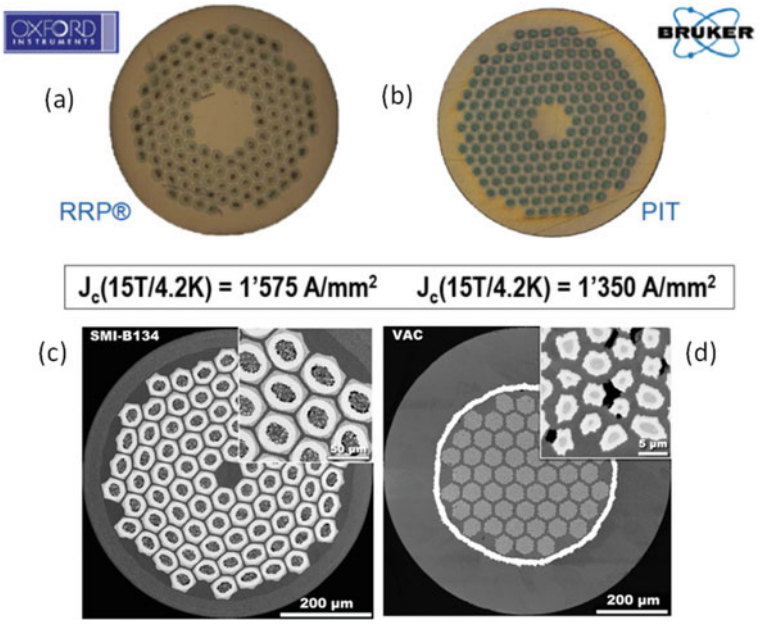

Fig. 14 Nb_3Sn wire development. **a** Restacked-rod process (RRP)-wires from Oxford Instruments (USA) and **b** PIT-wires from Bruker (Hanau, Germany). Reprinted from Ref. [107]. **c** Reinforced ternary PIT wire from SMI and **d** wires using the ternary bronze route from Vacuumschmelze (Hanau, Germany). Reprinted from Ref. [108]

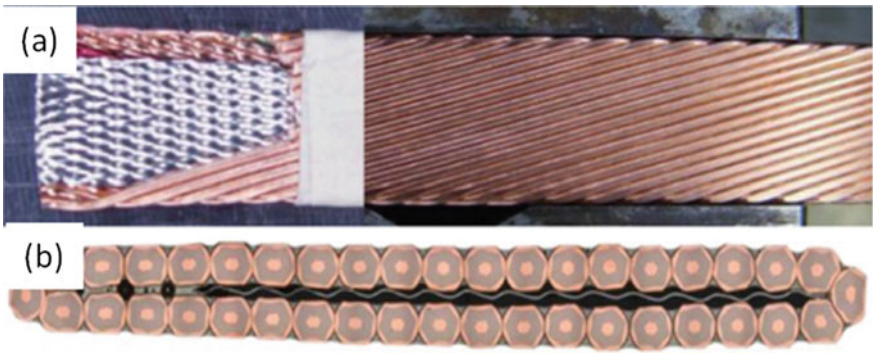

Fig. 15 Nb_3Sn Rutherford cables: **a** large face view of cable with stainless-steel (SS) core; **b** cross-sections of 40-strand cable. Reprinted from Ref. [109]

advantage of lower fabrication and material costs involved [111]. Wires of this type are manufactured by Plansee SE (Austria) [110].

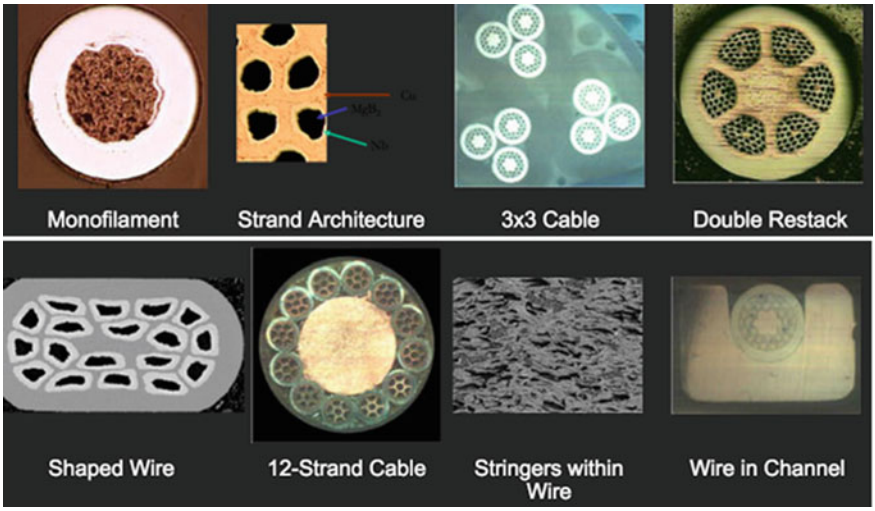

Fig. 16 MgB_2-wire development [109], showing the steps towards useful wire architecture

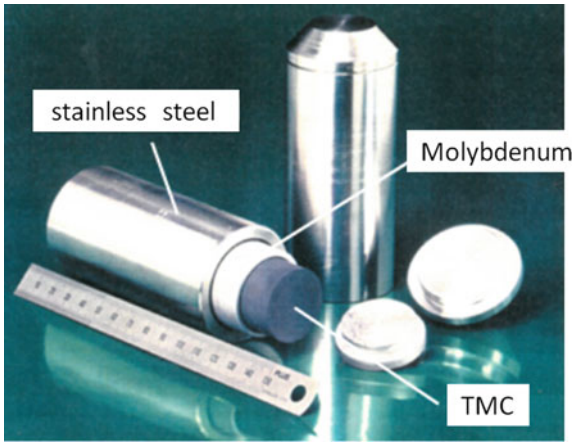

Fig. 17 Development of Chevrel-phase conductors of the TMC-type, showing an extrusion billet (~1.4 kg) for a 1 km long wire. Reinforcement by stainless steel is required for the foreseen high-field applications, Image from Plansee SE, courtesy B. Seeber [110]

5 Other Superconducting Materials

5.1 Heavy Fermions

The prerequisite for heavy fermion (HF) compounds is a high concentration of magnetic ions which build up periodic lattice sites. As consequence, it seemed to be remote to find superconductivity as the presence of strong magnetism prohibits in principle the formation of Cooper pairs. However, Steglich et al. [112] have found the superconductor $CeCu_2Si_2$, exhibiting unconventional superconductivity in ambient

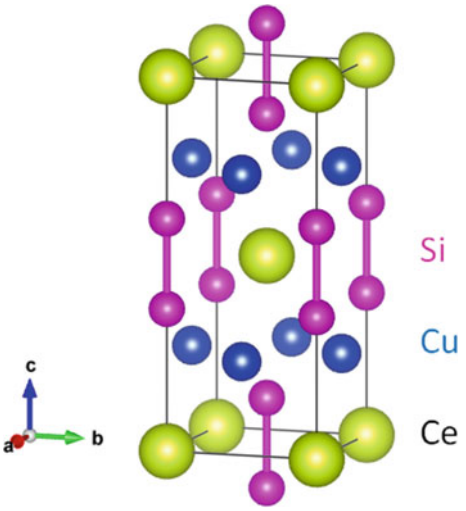

Fig. 18 Crystal structure of the heavy-fermion superconductor $CeCu_2Si_2$

conditions; the crystal structure is presented in Fig. 18. Since this time, superconductivity was discovered in more than 30 HF materials mainly containing Ce and U, and many more of their substituted phases, building up an entire class of materials with ferromagnetic and antiferromagnetic order. The superconductivity takes place mostly at T_c values below 2_K, but the most recently found materials $NpPd_5Al_2$ with $T_c = 4.9$ K [113] and $PuCoGa_5$ [114] with a T_c of even 18.5 K exhibit an even more strange behaviour (Table 5).

The unique properties of the HF superconductors were reviewed by Stewart [115] and Steglich [12, 116, 117]. Some superconducting parameters are listed in Table 4. The HF materials are strongly correlated materials with an effective charge carrier being 10—1000 larger than that of a free electron, with the direct consequence that the pairing mechanism is unconventional. These materials are still a big puzzle concerning the coexistence of magnetism and superconductivity [118], and so a recent article concludes that the superconducting state may arise due to the magnetism rather than in spite of it [119]. These observations on the HF systems, being classified

Table 5 Properties of selected heavy-fermion compounds. Data were collected from Refs. [12, 115]

Material	T_c (K)	Eff. mass (e_m)	B_{c2} (T)	λ_L (nm)	ξ_{GL} (nm)
URu_2Si	1.5	140	8	1000	10
$CeCu_2Si_2$	1.5	380	1.5–2.5	500	9
UPt_3	1.5	180	1.5	>1500	20
UBe_{13}	0.85	260	10	1100	9.5
UNi_2Al_3	1	48	<1	330	24
UPd_2Al_3	2	66	2.5–3	400	8.5

as unconventional superconductors, may also shed light on the pairing mechanism leading to high-T_c superconductivity (d-wave superconductivity), where a similar phase diagram with a coexistence of magnetism (antiferromagnetism) exists.

5.2 Borocarbides

At the same time as the Chevrel phases, ternary borides and stannides were discovered, all of which show also an interplay between magnetism and superconductivity. The formulae of these compounds are $RERh_4B_4$ (where RE = Nd, Sm, Er, or Tm) and the stannides are described by $RERh_xSn_y$ (where RE = La or Er with x ≈ 1–1.5 and y ≈ 3.5–4.5) [7]. The magnetic order in these materials can be ferromagnetic, antiferromagnetic, spin glass-type, oscillatory, as well as weakly ferromagnetic.

The most recent addition to this class of materials are the quaternary borides, which show an interplay with antiferromagnetism [3, 7]. The Ni-based borocarbides with the chemical formula $RENi_2B_2C$ (RE = Dy, Ho, Er, Tm, or Lu) exhibit superconducting transitions in the range between 6 and 17 K, with the most prominent member, YNi_2B_2C, becoming superconducting at 15.5 K (see Table 6). The T_c-value is found to increase up to 23 K, when Ni is replaced by Pd. The crystal structure (see Fig. 19) is body-centered tetragonal, with the electrical conduction taking place in the Ni_2B_2 layers. The T_c and the Néel temperature, T_N, values are very close to each other, exhibiting all possible combinations $T_c > T_N$, $T_c < T_N$, and $T_c \approx T_N$.

The superconducting properties in these compounds were reviewed in [120–123] and are considered as conventional superconductors, but similar to MgB_2, different energy bands contribute in different fashion to superconductivity. Borocarbides are type-2 superconductors with $\kappa \sim 15$ ($\xi \sim 10$ nm, $\lambda \sim 150$ nm and B_{c2} up to 10_T). Furthermore, in this family also antiferromagnetism and superconductivity can coexist, with the compound $YbNi_2B_2C$ exhibiting a heavy-fermion behavior. Furthermore, it was shown in [124] that the grain boundaries of polycrystalline borocarbide samples act as weak links like in the case of the HTSc cuprates, which makes them uninteresting for possible applications.

Table 6 Properties of selected borocarbide compounds. Data were collected from Refs. [3, 120–123]

Material	T_c (K)	B_{c2} (T)	λ_L (nm)	ξ_{GL} (nm)
YPd_2B_2C	23	–	–	–
$LuNi_2B_2C$	16.6	7	70–130	7
YNi_2B_2C	15.5	6.5	120–350	6.5
$TmNi_2B_2C$	11	–	–	–
$ErNi_2B_2C$	10.5	1.4	750	15
$HoNi_2B_2C$	7.5	–	–	–

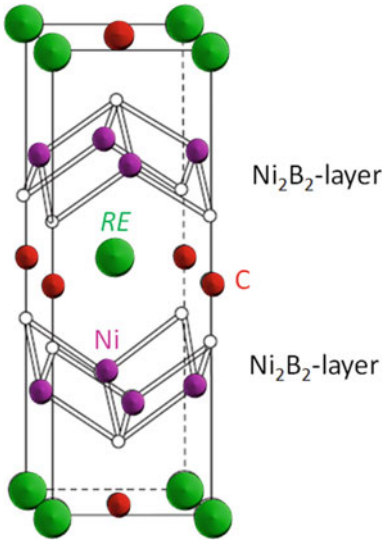

Fig. 19 Crystal structure of the quarternary borocarbide $RENi_2B_2C$ (RE = rare earths)

5.3 *Layered Superconductors*

The thin film preparation technology enabled the growth of multilayered systems consisting of, e.g., a metal and a superconductor, an insulator and a superconductor or two superconductors with different superconducting properties. As the thicknesses of the constituents can be varied, artificial multilayers with a variety of properties can be fabricated. Such materials were reviewed in [125, 126]. Even more interesting are materials with an internal layer structure or real 2D superconductors. If the coherence length gets smaller than the interlayer distance, the superconducting state will vary spatially, and in the extreme case, there will be an atomic sequence of superconducting and non-superconducting layers, where superconducting current perpendicular to the layers will flow as Josephson currents. Beginning in the 1960s, such natural layered superconductors were investigated. The general formula of these systems can be written as MX_2 with M being a transition metal and X a chalcogenide Se, S or Te [3, 7]. A typical crystal structure of this material class is shown in Fig. 20 for the case of niobium diselenide ($NbSe_2$), which was described first in [127].

This material is very interesting for low-temperature STM investigations as a calibration material, as the structure can readily be cleaved. With the upcoming of van der Waals-coupled multilayer engineering [128, 129], $NbSe_2$ is best suited to provide a superconducting contribution for such 2D-vdW-architectures.

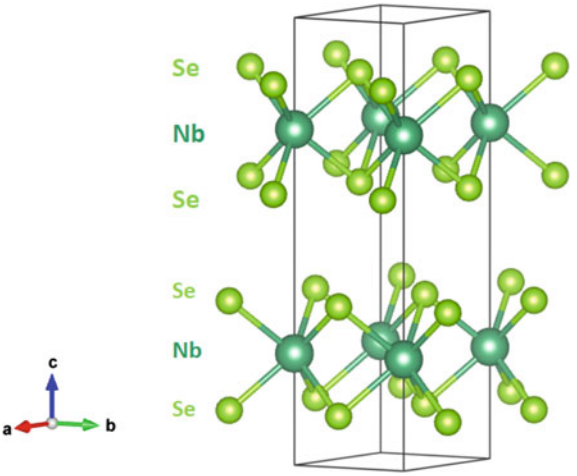

Fig. 20 Crystal structure of $NbSe_2$ as an example of layered or 2D-superconductors

6 New Developments

6.1 New Materials

New superconducting materials are still searched for, and the Matthias' rule is still an important guide to do so [130]. Recently, the Matthias' rules helped to find a new class of superconductors, which crystallize in the $AuCu_3$-type lattice, that is, the compounds of $LaBi_3$ [19]. The finding of superconducting high-entropy alloys is also strongly guided by the valence electron count, *e*/a. This demonstrates that there are still many more superconducting materials to discover, and the help of machine learning to search databases and to perform band structure calculations [21–23] will certainly contribute to these efforts in the future.

6.2 High-Entropy Alloys (HEA) Compounds

A new field for research opened up when the high-entropy alloys (HEA) were found to contain also superconducting members. Based on the overall structure of the Nb-Ti-system, a total of 5 elements were composed to achieve the HEA effect as illustrated in Fig. 21. All atoms may occupy any lattice site with the same probability. The first such alloy was $Ta_{34}Nb_{33}Ti_{11}Zr_{14}Hf_8$, found by Kozelj et al. [20] with a T_c of 7.3 K. The basic idea of the HEA compound is depicted in Fig. 20. All atoms involved may take any position in the unit cell, in this case a *bcc* one. In the meantime, other HEA compounds including Nb-Re-Hf-Zr-Ti, Hf-Nb-Ti-V-Zr, Mo-Re-Ru-Rh-Ti [131, 132] and such containing U were found to be superconductors [133].

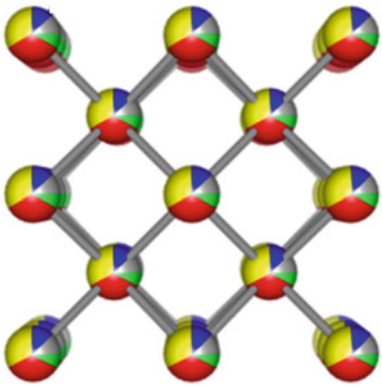

Fig. 21 Composition scheme of the HEA alloys in the *bcc* structure. All atoms involved may occupy each lattice site as indicated by the different colors

It was later shown that HEA is not limited to the *bcc* unit cell as a superconducting hexagonal HEA alloy ($Re_{56}Nb_{11}Ti_{11}Zr_{11}Hf_{11}$) with a T_c of 4.4 K was found [134], and the HEA $AgInSnPbBiTe_5$ crystallizes in a NaCl-structure (space group Fm-3 m), with the metals on the cation site and Te on the anion site. The T_c of this system is 2.8 K [135]. V-Nb-Mo-Al-Ga shows polymorphism and crystallizes for some mixing ratio in the bcc structure but upon annealing, an A15-structure is obtained [136].

While in the A15-structure, the highest upper critical field for all HEAs of 20.1 T was measured. All the superconducting HEAs are type-2 superconductors with critical fields up to 8–10 T. The remarkable behavior of the electron system of the HEA compounds became visible in high-pressure experiments as shown in Fig. 6, which indicates that the electronic character of the HEA is different from that of the single constituents. The consequences this may have for the fabrication of wires is still not yet explored. Thus, there will be for sure more interesting physics coming out from such systems in the future.

6.3 Magic-Angle Bi-layered Graphene

Carbon becomes superconducting in various forms, including the carbon-doped diamond films and carbon nanotubes [30, 31]. Another interesting carbon material is graphene, and superconductivity in such systems was discovered recently in magic-angle, twisted bi-layered graphene (MA-tblG) [32–34]. Placing two graphene layers together under an angle of 1.1° forms a Moiré pattern as shown in Fig. 22. This observation leads to a new type of superconducting material, being the start of the so-called Moiré superconductivity, where superconductivity depends on the Moiré pattern formed between two or more atomically flat layers with a much larger lattice parameter. The T_c of MA-tblG is low with T_c ranging between 0.5 and 1.4 K, but it could be shown that adding hexagonal boron nitride (h-BN) layers of different thickness improves T_c up to 4 K [34].

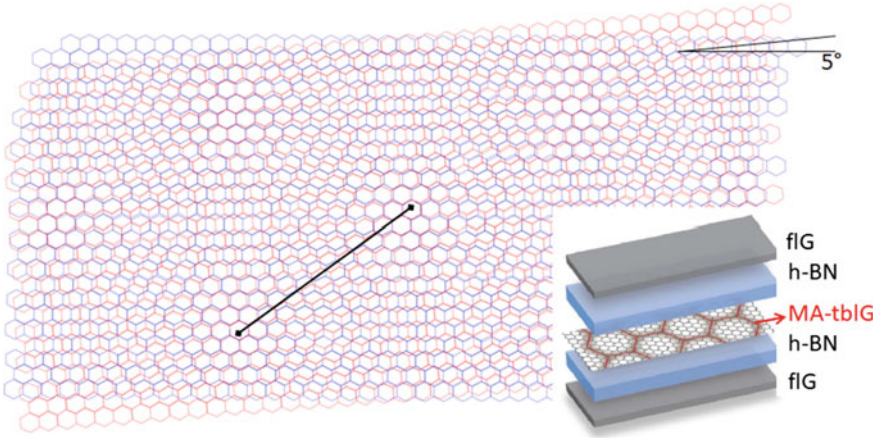

Fig. 22 Magic-angle bi-layered graphene (MA-tblG), presented as Moiré-pattern of two 5°-tilted graphene layers for clarity. The bold line shows the new Moiré lattice parameter. The inset presents the arrangement for measurements, where the sample is covered by few layers of graphite flakes (flG) acting as gates

The superconductivity of the MA-tblG layers is on the way to be understood in detail [137], even though more careful experiments on the Moiré superconductors, which include also other 2D-layers with similar structure like e.g., WSe_2 [138], regarding their superconducting properties are still required.

6.4 Metal Hydrides Under Pressure

Superconductivity in metal-hydrides was found in 1972 by Skoskiewicz in the Pd-H system [139]. A maximum T_c of ~4 K was obtained for a ratio H/Pd ~ 0.9 in ambient conditions. However, if the pressure is sufficiently high, hydrogen is believed to become a monatomic metal with exotic electronic properties owing to the quantum nature of this low-Z system [28, 140]. Due to the fact that very high pressures are required to create such states, hydrogen-rich metal compounds, in which the hydrogen is chemically pre-compressed, have been considered as an alternative for experimental work.

In recent experiments, X-ray diffraction and optical studies have demonstrated that super-hydrides of lanthanum can be synthesized with La atoms in an *fcc* lattice at 170 GPa upon heating to about 1000 K. The results obtained in [27, 141, 142] match the predicted cubic metallic phase of LaH_{10} [143] having cages of thirty-two hydrogen atoms surrounding each La atom. This configuration is up to now the closest one to pure metallic hydrogen. Four-probe electrical transport measurements were

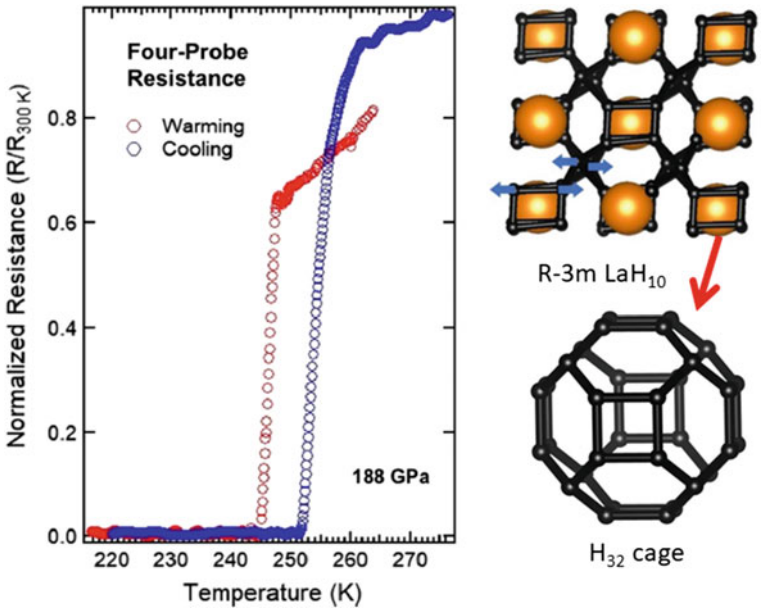

Fig. 23 Resistance measurements under high pressure (188 GPa) on LaH_{10}.Reproduced with permission from Ref. [141]. On the right, the crystal structure of R-3 m-LaH_{10} is shown, with the blue arrows indicating displacements of the H-cluster. Below the H_{32}-cluster which surrounds each La atom in the structure is presented. Reproduced with permission from Ref. [143]

performed in the high-pressure environment that display significant drops in resistivity on cooling up to 260 K and 180–200 GPa. These measured transitions represent signatures of superconductivity at near room temperature, which is a remarkable result, initiating a new area in superconductivity [42]. The underlying mechanism is, however, that of conventional superconductivity based on electron–phonon interaction (Fig. 23).

7 Conclusion

The conventional or low-T_c superconductors are by no means dead as one could think during the hype around the various high-T_c materials: The LTSc still serve as model systems in basic physics, e.g., for creating mesoscopic superconducting samples, 2D superconductors or model systems to investigate flux pinning properties. Concerning the fabrication of superconducting wires, there is still a lot of development required to design and produce the wires and cables for the current big projects like ITER and the planned fusion reactors. And, very important, there are new and unexpected results reported in the literature, which give the entire field a new push. This concerns mainly the discovery of new superconducting materials like

the discovery of the high-entropy alloys (HEA), which was based on the Matthias' rules. These materials show up with interesting new properties. This is especially the case for the high-pressure dependence of T_c, which exhibited superconductivity up to 190 GPa pressure. This result points out that the electron system of a HEA is truly different from its individual components like No or Ta. Very remarkably, it was found that the parent compound of the HEA, NbTi, was never investigated before at high pressures, carrying out this experiment recently, brought out the striking result that T_c of NbTi can be increased up to 19 K, and the superconductivity persists also up to 261 GPa, the highest pressure which can be applied experimentally. Furthermore, superconductivity was found in magic-angle, bi-layered graphene, creating a new class of superconducting materials, the Moiré-type superconductors. And, the high-pressure experiments on LaH_{10} reaching room-temperature superconductivity put the research on metallic superconductors to the forefront of interest. Thus, there is a lot of exciting new physics in this field, coming up certainly with new and important results in the near future.

References

1. H.K. Onnes, The superconductivity of mercury. Commun. Phys. Lab. Univ. Leiden 120b, 122b, 124c (1911)
2. D. van Delft, P.H. Kes, The discovery of superconductivity. Phys. Today **63**, 38–43 (2010)
3. W. Buckel, R. Kleiner, *Supraleitung. Grundlagen und Anwendungen,* 7th edn. (Wiley-VCH, Weinheim, 2013)
4. B. Seeber (ed.), *Handbook of Applied Superconductivity* (IOP Publishing, Bristol, UK, 1999)
5. D.A. Cardwell, D.S. Ginley (eds.), *Handbook of Superconducting Materials* (CRC Press, Boca Raton, USA, 2002)
6. P. Seidel (ed.), *Applied Superconductivity* (Wiley-VCH, Weinheim, Germany, 2015)
7. A.V. Narlikar, *Superconductors* (Oxford University Press, Oxford, U.K., 2014)
8. K.H. Bennemann, J.B. Ketterson (eds.), *Superconductivity* (Springer, Berlin, Heidelberg, Germany, 2008)
9. B.T. Matthias, Chapter V superconductivity in the periodic system. Prog. Low Temp. Phys. **2**, 138–150 (1957)
10. B.T. Matthias, T.H. Geballe, V.B. Compton, Superconductivity. Rev. Mod. Phys. **35**, 1–22 (1963)
11. J.R. Gavaler, M.A. Janocko, C.K. Jones, Preparation and properties of high T_c Nb-Ge thin films. J. Appl. Phys. **45**, 3009–3012 (1974)
12. R. Chevrel, M. Sergent, J. Prigent, Sur de nouvelles phases sulfurées ternaires du molybdène. J. Solid State Chem. **3**, 515–519 (1971)
13. F. Steglich, S. Wirth, Foundations of heavy-fermion superconductivity: lattice Kondo effect and Mott physics. Rep. Prog. Phys. **79**, 084502 (2016)
14. H. Takagi, M. Nohara, R.J. Cava, Borocarbide superconductors: materials and physical properties. Phys. B **237–238**, 292–295 (1997)
15. K.A. Müller, J.G. Bednorz, Possible high T_c superconductivity in the Ba-La-Cu-O system. Z. Phys. B **64**, 189–193 (1986)
16. J. Nagamatsu, N. Nakagawa, T. Muranaka, Y. Zenitani, J. Akimitsu, Superconductivity at 39 K in magnesium diboride. Nature **410**, 63–64 (2001)
17. A. Bezryadin, *Superconductivity in Nanowires* (Wiley-VCH, Weinheim, Germany, 2013)

18. F. Altomare, A.M. Chang, *One-Dimensional Superconductivity in Nanowires* (Wiley-VCH, Weinheim, Germany, 2013)
19. T. Kinjo, S. Kajino, T. Nishio, K. Kawashima, Y. Yanagi, I. Hase, T. Yanagisawa, S. Ishida, H. Kito, N. Takeshita, K. Oka, H. Eisaki, Y. Yoshida, A. Iyo, Superconductivity in $LaBi_3$ with $AuCu_3$-type structure. Supercond. Sci. Technol. **29**, 03LT02 (2016)
20. P. Kozelj, S. Vrtnik, A. Jelen, S. Jazbec, Z. Jaglicic, S. Maiti, M. Feuerbacher, W. Steurer, J. Dolinsek, Discovery of a superconducting HEA alloy. Phys. Rev. Lett. **113**, 107001 (2014)
21. K. Matsumoto, T. Horide, An acceleration search method of higher T_c superconductors by a machine learning algorithm. Appl. Phys. Express **12**, 073003 (2019)
22. M.J. Hutcheon, A.M. Shipley, R.J. Needs, Predicting novel superconducting hydrides using machine learning approaches. Phys. Rev. B **101**, 144505 (2020)
23. S. Zeng, Y. Zhao, G. Li, R. Wang, X. Wang, J. Ni, Atom table convolutional neural networks for an accurate prediction of compounds properties. npj Comput. Mater. **5**, 84 (2019)
24. J. Guo, H. Wang, F. von Rohr, Z. Wang, S. Cai, Y. Zhou, K. Yang, S. Jiang, Q. Wu, R.J. Cava, L. Sun, Robust zero resistance in a superconducting high-entropy alloy at pressures up to 190 GPa. Proc. Nat. Acad. Sci. **114**, 13144–13147 (2017)
25. J. Guo, G. Lin, S. Cai, C. Xi, C. Zhang, W. Sun, Q. Wang, K. Yang, A. Li, Q. Wu, Y. Zhang, T. Xiang, R.J. Cava, L. Sun, Record-high superconductivity in Niobium-Titanium alloy. Adv. Mater. **31**, 1807240 (2019)
26. A.P. Drozdov, M.I. Eremets, I.A. Troyan, V. Ksenofontov, S.I. Shylin, Conventional superconductivity at 203 kelvin at high pressures in the sulfur hydride system. Nature **525**, 73–76 (2015)
27. A.P. Drozdov, P.P. Kong, V.S. Minkov, S.P. Besedin, M.A. Kuzovnikov, S. Mozaffari, L. Balicas, F.F. Balakirev, D.E. Graf, V.B. Prakapenka, E. Greenberg, D.A. Knyazev, M. Tkacz, M.I. Eremets, Superconductivity at 250 K in lanthanum hydride under high pressures. Nature **569**, 528–533 (2019)
28. N.W. Ashcroft, Metallic hydrogen: a high- temperature superconductor? Phys. Rev. Lett. **21**, 1748–1749 (1968)
29. K.J.B. Ghosh, S. Kais, D.R. Herschbach, Dimensional interpolation for metallic hydrogen. Phys. Chem. Chem. Phys. **23**, 7841–7848 (2021)
30. Z.K. Tang, L. Zhang, N. Wang, X.X. Zhang, G.H. Wen, G.D. Li, J.N. Wang, C.T. Chen, P. Sheng, Superconductivity in 4 angstrom single-walled carbon nanotubes. Science **292**, 2462–2465 (2001)
31. A. Bhaumik, R. Sachan, J. Narayan, High-temperature superconductivity in boron-doped Q-carbon. ACS Nano **11**, 5351–5357 (2017)
32. Y. Cao, V. Fatemi, S. Fang, K. Watanabe, T. Taniguchi, E. Kaxiras, P. Jarillo-Herrero, Unconventional superconductivity in magic-angle graphene superlattices. Nature **556**, 43–50 (2018)
33. M. Yankowitz, S. Chen, H. Polshyn, Y. Zhang, K. Watanabe, T. Taniguchi, D. Graf, A.F. Young, C.R. Dean, Tuning superconductivity in twisted bilayer graphene. Science **363**, 1059–1064 (2019)
34. Y. Saito, J. Ge, K. Watanabe, T. Taniguchi, A.F. Young, Independent superconductors and correlated insulators in twisted bilayer graphene. Nature Phys. **16**, 926–930 (2020)
35. M. Sawabu, M. Ohashi, K. Ohashi, M. Miyagawa, T. Kubota, K. Takanashi, The electrical resistivity of epitaxially deposited chromium films. IOP Conf. Ser. **871**, 012002 (2017)
36. B. Stritzker, Superconductivity in irradiated palladium. Phys. Rev. Lett. **41**, 1769–1773 (1979)
37. O. Prakash, Anil Kumar, A. Thamizhavel, S. Ramakrishnan, Evidence for bulk superconductivity in pure bismuth single crystals at ambient pressure. Science **355**, 52–55 (2017)
38. J. Tuoriniemi, K. Juntunen-Nurmilaukas, J. Uusvuori, E. Pentti, A. Salmela, and A. Sebedash, Superconductivity in lithium below 0.4 millikelvin at ambient pressure. Nature **447**, 187–189 (2007)
39. K. Shimizu, T. Kimura, S. Furomoto, K. Takeda, K. Kontani, Y. Onuki, K. Amaya, Superconductivity in the non-magnetic state of iron under pressure. Nature **412**, 316–318 (2001)

40. K. Schwochau, *Technetium: Chemistry and Radiopharmaceutical Applications* (Wiley-VCH, Weinheim, Germany, 2000)
41. C. Buzea, K. Robbie, Assembling the puzzle of superconducting elements: a review. Supercond. Sci. Technol. **18**, R1–R8 (2005)
42. J.A. Flores-Livas, L. Boeri, A. Sanna, G. Profeta, R. Arita, M. Eremets, A perspective on conventional high-temperature superconductors at high pressure: methods and materials. Phys. Rep. **856**, 1–78 (2020)
43. M. Debessai, T. Matsuoka, J.J. Hamlin, J. S. Schilling, K. Shimizu, Pressure-induced superconducting state of Europium metal at low temperatures. Phys. Rev. Lett. **102**, 197002 (2009)
44. H.P. Roeser, D.T. Haslam, J.S. Lopez, M. Stepper, M.F. von Schoenermark, F.M. Huber, A.S. Nikoghosyan, Correlation between transition temperature and crystal structure of niobium, vanadium, tantalum and mercury superconductors. Acta Astronaut. **67**, 1333–1336 (2010)
45. M.R. Koblischka, S. Roth, A. Koblischka-Veneva, T. Karwoth, A. Wiederhold, X.L. Zeng, S. Fasoulas, M. Murakami, Relation between crystal structure and transition temperature of superconducting metals and alloys. Metals **10**, 158 (2020)
46. A. Moritz, Calculation of the transition temperature of one-component-superconductors (in German). Master thesis IRS 09-S33, Institute of Space Systems, University of Stuttgart, Stuttgart, Germany (2009)
47. M. Stepper, Calculation of the transition temperature of two-component-superconductors (in German). Master thesis IRS 08-S23, Institute of Space Systems, University of Stuttgart, Stuttgart, Germany (2008)
48. K. Momma, F. Izumi, VESTA 3 for three-dimensional visualization of crystal, volumetric and morphology data. J. Appl. Crystallogr. **44**, 1272–1276 (2011)
49. ICDD PDF Data Base, ICDD: 12 Campus Blvd, Newtown Square, PA 19073, USA. Accessed 22 Aug 2021
50. Materials Project Database V2019.05. https://materialsproject.org/. Accessed 22 Aug 2021
51. Crystallography Open Database (COD). http://www.crystallography.net/cod/. Accessed 22 Aug 2021
52. R.W. Cohen, B. Abeles, Superconductivity in granular aluminum films. Phys. Rev. **168**, 444–450 (1968)
53. Y. Ivry, C.-S. Kim, A.E. Dane, D. De Fazio, A.N. McCaughan, K.A. Sunter, Q. Zhao, K. Berggren, Universal scaling of the critical temperature for thin films near the superconducting-to-insulating transition. Phys. Rev. B **90**, 214515 (2014)
54. Y. Guo, Y.-F. Zhang, X.J. Bao, T.Z. Han, Z. Tang, L.X. Zhang, W.G. Zhu, E. Wang, Q. Niu, Z.Q. Qiu, J.-F. Jia, Q.-K. Xue, Superconductivity modulated by quantum size effects. Science **306**, 1915–1917 (2004)
55. M. Zgirski, K.P. Riikonen, V. Touboltsev, K. Arutyunov, Size dependent breakdown of superconductivity in ultranarrow nanowires. Nano Lett. **50**, 1029–1033 (2005)
56. K.O. Moura, K.R. Pirota, F. Béron, C.B.R. Jesus, P.F.S. Rosa, D. Tobia, P.G. Pagliuso, O.F. de Lima, Superconducting properties in arrays of nanostructured β-gallium. Sci. Rep. **7**, 15306 (2017)
57. W.J. de Haas, J. Voogd, On the superconductivity of the gallium. Commun. Phys. Lab. Univ. Leiden **199d**, 733–734 (1929)
58. B.W. Roberts, Survey of superconductive materials and critical evaluation of selected properties. J. Phys. Chem. Ref. Data **5**, 581–821 (1976)
59. M.R. Koblischka, A. Koblischka-Veneva, Fabrication of superconducting nanowires using the template method. Nanomaterials **11**, 1970 (2021)
60. G. Aschermann, E. Friedrich, E. Justi, J. Kramer, Superconductive connections with extremely high cracking temperatures (NbH and NbN). Phys. Z. **42**, 349–360 (1941)
61. G. Horn, E. Saur, Preparation and superconductive properties of niobium nitride and niobium nitride with admixtures of titanium, zirconium and tantalum. Z. Phys. **210**, 70–79 (1968)
62. H. Rögener, Zur Supraleitung des Niobnitrids. Z. Phys. **132**, 446–467 (1952)

63. K. Hechler, G. Horn, G. Otto, E. Saur, Measurements of critical data for some type II superconductors and comparison with theory. J. Low Temp. Phys. **1**, 29–43 (1969)
64. S. Leith, M. Vogel, J. Fan, E. Seiler, R. Ries, and X. Jiang, Superconducting NbN thin films for use in superconducting radio frequency cavities. Supercond. Sci. Technol. **34**, 025006 (2021)
65. L. You, Superconducting nanowire single-photon detectors for quantum information. Nanophotonics **9**, 2673–2692 (2020)
66. S. Steinhauer, S. Gyger, and V. Zwiller, Progress on large-scale superconducting nanowire single-photon detectors. Appl. Phys. Lett. **118**, 100501 (2021)
67. B.A. Glowacki, Development of Nb based conductors, in *Frontiers of Superconducting Materials*. ed. by A.V. Narlikar (Springer, Berlin, Heidelberg, Germany, 2005), pp. 697–738
68. D. Gajda, Analysis method of high-field pinning centers in NbTi wires and MgB_2 wires. J. Low Temp. Phys. **194**, 166–182 (2019)
69. C. Meingast, D.C. Larbalestier, Quantitative description of a very high critical current-density Nb-Ti superconductor during its final optimization strain. 2. Flux pinning mechanism. J. Appl. Phys. **66**, 5971–5983 (1989)
70. T.S. Hutchinson, G. Ocampo, G.J.C. Carpenter, Crystal structure and morphology in commercial NbTi (46.5 wt.-% Ti) superconducing fibers. Scr. Metall. **19**, 635–638 (1985)
71. M.C. Steele, R.A. Hein, Superconductivity of titanium. Phys. Rev. **92**, 243–247 (1953)
72. H. Hillmann, Interaction of metallurgical treatment and flux pinning of NbTi superconductors. Supercond. Sci. Technol. **12**, 348–355 (1999)
73. J. Shimizu, K. Tonooka, Y. Yoshida, M. Furuse, H. Takashima, Growth and superconductivity of niobium titanium alloy thin films on strontium titanate (001) single crystal substrates for superconducting joints. Sci. Rep. **8**, 15135 (2018)
74. G.F. Hardy, J.K. Hulm, The superconductivity of some transition metal compounds. Phys. Rev. **93**, 1004–1016 (1954)
75. B.T. Matthias, T.H. Geballe, S. Geller, E. Corenzwit, Superconductivity of Nb_3Sn. Phys. Rev. **95**, 1435
76. G.A. Stewart, Superconductivity in the A15 structure. Phys. C **514**, 28–35 (2015)
77. B.T. Matthias, T.H. Geballe, L.D. Longinotti, E. Corenzwit, G.W. Hull, R.H. Willens, J.P. Maita, Superconductivity at 20 degrees Kelvin. Science **156**, 645–646 (1967)
78. G.W. Webb, L.J. Vieland, R.E. Miller, A. Wicklund, Superconductivity above 20 degrees K in stoichiometric Nb_3Ga. Solid State Commun. **9**, 1769–1773 (1971)
79. L.R. Testardi, J.H. Wernick, W.A. Royer, Superconductivity with onset above 23 K in Nb-Ge sputtered films. Solid State Commun. **15**, 1–4 (1974)
80. Y. Hishinuma, H. Taniguchi, A. Kikuchi, Development of the internal matrix reinforcement bronze processed Nb_3Sn multicore wires using Cu-Sn-In ternary alloy matrix for fusion magnet application. Fusion Eng. Des. **148**, 111269 (2019)
81. S. Kawashima, T. Kawarada, H. Kato, Y. Murakami, M. Sugano, H. Oguro, S. Awaji, Development of a high current density distributed Tin method Nb_3Sn wire. IEEE Trans. Appl. Supercond. **30**, 6000105 (2020)
82. A. Ballarino, S.C. Hopkins, C. Simon, B. Bordini, D. Richter, D. Tommasini, L. Bottura, M. Benedikt, M. Sugano, T. Ogitsu, S. Kawashima, K. Saito, Y. Fukumoto, H. Sakamoto, H. Shimizu, V. Pantsyrny, I. Abdyukhanov, M. Shlyakov, S. Zernov, F. Buta, C. Senatore, I. Shin, J. Kim, J. Lachmann, A. Leineweber, S. Pfeiffer, T. Baumgartner, M. Eisterer, J. Bernardi, A. Malagoli, V. Braccini, M. Vignolo, M. Putti, C. Ferdeghini, The CERN FCC conductor development program: a worldwide effort for the future generation of high-field magnets. IEEE Trans. Appl. Supercond. **29**, 6000709 (2019)
83. J.R. Gavaler, M.A. Janocko, C.K. Jones, Preparation and properties of high-T_c Nb-Ge thin films. J. Appl. Phys. **45**, 3009–3012 (1974)
84. M.N. Sayeed, U. Pudasaini, C.E. Reece, G. Eremeev, H.E. Elsayed-Ali, Structural and superconducting properties of Nb_3Sn films grown by multilayer sequential magnetron sputtering. J. Alloys Compounds **800**, 272–278 (2019)

85. R. Chevrel, M. Hirrien, M. Sergent, Superconducting Chevrel phases: prospects and perspectives. Polyhedron **5**, 87–94 (1986)
86. B.T. Matthias, M. Marezio, E. Corenzwit, A.S. Cooper, H.E. Barz, High-temperature superconductors, the first ternary system. Science **175**, 1465–1466 (1972)
87. Ø. Fischer, A. Treyvaud, R. Chevrel, M. Sergent, Superconductivity in the $RE_xMo_6S_8$. Solid State Commun. **17**, 721–724 (1975)
88. R. Odermatt, Ø. Fischer, H. Jones, G. Bongi, Upper critical fields of some ternary molybdenum sulphides. J. Phys. **C7**, L13–L15 (1974)
89. S. Foner, E.J. McNiff Jr., E.J. Alexander, 600 kG superconductors. Phys. Lett. **49A**, 269–270 (1974)
90. B. Seeber, N. Cheggour, J.A.A.J. Perenboom, R. Grill, Critical current distribution of hot isostatically pressed $PbMo_6S_8$ wires. Physica C **234**, 343–354 (1994)
91. B. Seeber, M. Decroux, O. Fischer, Status and prospects of superconducting Chevrel phase wires for high magnetic field applications. Physica B **155**, 129–135 (1989)
92. C. Buzea, T. Yamashita, Review of the superconducting properties of MgB_2. Supercond. Sci. Technol. **14**, R115–R146 (2001)
93. T. Muranaka, J. Akimitsu, Superconductivity in MgB_2. Z. Kristallogr. **226**, 385–394 (2011)
94. S. Souma, Y. Machida, T. Sato, T. Takahashi, H. Matsui, S.-C. Wang, H. Ding, A. Kaminski, J. C.. Campuzano, S. Sasaki, K. Kadowaki, The origin of multiple superconducting gaps in MgB_2. Nature **423**, 65–67 (2003)
95. M. Kambara, N. Hari Babu, E.S. Sadki, J.R. Cooper, H. Minami, D.A. Cardwell, A.M. Campbell, I.H. Inoue, High intergranular critical currents in metallic MgB_2 superconductor. Supercond. Sci. Technol. **14**, L5–L7 (2001)
96. P. Mikheenko, E. Martinez, A. Bevan, J.S. Abell, J.L. MacManus-Driscoll, Grain boundaries and pinning in bulk MgB_2. Supercond. Sci. Technol. **20**, S264–S272 (2007)
97. K.D. Belashenko, M. van Schilfgaarde, V.P. Antropov, Coexistence of covalent and metallic bonding in the boron intercalation superconductor MgB_2. Phys. Rev. B **64**, 092503 (2001)
98. S.K. Das, A. Bedar, A. Kannan, K. Jasuja, Aqueous dispersions of few-layer-thick chemically modified magnesium diboride nanosheets by ultrasonication assisted exfoliation. Sci. Rep. **5**, 10522 (2015)
99. I. Pallecchi, V. Ferrando, E. Galleani D'Agliano, D. Marré, M. Monni, M. Putti, C. Tarantini, F. Gatti, H.U. Aebersold, E. Lehmann, X.X. Xi, E.G. Haanappel, C. Ferdeghini, Magnetoresistivity as a probe of disorder in the π and σ bands of MgB_2. Phys. Rev. B **72**, 184512 (2005). Erratum in Phys. Rev. B **73**, 029901 (2006)
100. R.S. Gonnelli, D. Daghero, G.A. Ummarino, V.A. Stepanov, J. Jun, S.M. Kazakov, J. Karpinski, Direct evidence for two-band superconductivity in MgB_2 single crystals from directional point-contact spectroscopy in magnetic fields. Phys. Rev. Lett. **89**, 247004 (2002)
101. V. Moshchalkov, M. Menghini, T. Nishio, Q.H. Chen, A.V. Silhanek, V.H. Dao, L.F. Chibotaru, N.D. Zhigadlo, J. Karpinski, Type-1.5 superconductivity. Phys. Rev. Lett. **102**, 117001 (2009)
102. A. Ballarino, R. Flükiger, Status of MgB_2 wire and cable applications in Europe. J. Phys. Conf. Ser. **871**, 012098 (2017)
103. H. ten Kate, ESIPAP-CERN lecture, https://indico.cern.ch/event/301339/contributions/688973/attachments/568795/783412/TenKate_-_ESIPAP_-_Lecture_1_-_Superconductors_for_Magnets_3Mar14.pdf. Accessed 22 Aug 2021
104. P.J. Lee, https://fs.magnet.fsu.edu/~lee/plot/plot.htm. Accessed 22 Aug 2021
105. A. Godeke, A. den Ouden, A. Nijhuis, H.H.J. ten Kate, State of the art powder-in-tube niobium–tin superconductors. Cryogenics **48**, 308–316 (2008)
106. E. Barzi, A.V. Zlobin, in *Nb_3Sn Accelerator Magnets Designs, Technologies and Performance* ed. by D. Schoerling, A.V. Zlobin (Springer Open, Cham, Switzerland, 2019), p. 39
107. R. Flükiger, Superconductivity for magnets, in *Proceedings of the CAS–CERN Accelerator School: Superconductivity for Accelerators*, Erice, Italy, 24 April–4 May 2013, ed. by R. Bailey, CERN-2014–005 (CERN, Geneva, 2014), pp. 247–267
108. A. Godeke, Performance boundaries in Nb_3Sn superconductors. PhD thesis, University of Twente, Enschde, The Netherlands (2005)

109. https://www.nextbigfuture.com/2015/08/magnesium-diboride-superconductors-can.html. Accessed 22 Aug 2021
110. R. Grill, E. Kny, B. Seeber, Anwendung von Refraktärmetallen in Keramik Supraleiter, in *Proceedings of 12th Plansee Seminar*, Reutte, Austria (1989), pp. 989–1006
111. B. Seeber, Ternary molybdenum chalcogenide superconducting wires for ultrahigh field applications. IEEE Trans. Appl. Supercond. **28**, 6900305
112. F. Steglich, J. Aarts, C.J. Bredl, W. Lieke, D. Meschede, W. Franz, H. Schäfer, Phys. Rev. Lett. **43**, 1892–1895 (1979)
113. D. Aoki, A. Nakamura, F. Honda, D. Li, Y. Homma, Y. Shimizu, Y.J. Sato, G. Knebel, J. Brison, A. Pourret, D. Braithwaite, G. Lapertot, Q. Niu, M. Vališka, H. Harima, J. Flouquet, Unconventional superconductivity in heavy fermion UTe_2. J. Phys. Soc. Jpn. **88**, 043702 (2019)
114. J.L. Sarrao, L.A. Morales, J.D. Thompson, B.L. Scott, G.R. Stewart, F. Wastin, J. Rebizant, P. Boulet, E. Colineau, G.H. Lander, Plutonium-based superconductivity with a transition temperature above 18 K. Nature **420**, 297–299 (2002)
115. G.R. Stewart, Heavy-fermion systems. Rev. Mod. Phys. **56**, 755–787 (1984)
116. F. Steglich, J. Arndt, S. Friedemann, C. Krellner, Y. Tokiwa, T. Westerkamp, M. Brando, P. Gegenwart, C. Geibel, S. Wirth, O. Stockert, Superconductivity versus quantum criticality: what can we learn from heavy fermions? J. Phys. Cond. Mat. **22**, 164202 (2010)
117. F. Steglich, O. Stockert, S. Wirth, C. Geibel, H. Q. Yuan, S. Kirchner, Q. Si, Routes to heavy-fermion superconductivity. J. Phys. Conf. Ser. **449**, 012028 (2013)
118. A. Amato, E. Bauer, C. Baines, On the coexistence magnetism/superconductivity in the heavy-fermion superconductor $CePt_3Si$. Phys. Rev. B **71**, 092501 (2005)
119. N.D. Mathur, F.M. Grosche, S.R. Julian, I.R. Walker, D.M. Freye, R.K.W. Haselwimmer, G.G. Lonzarich, Magnetically mediated superconductivity in heavy fermion compounds. Nature **394**, 39–43 (1998)
120. C. Mazumdar, R. Nagarajan, C. Godart, L.C. Gupta, M. Latroche, S.K. Dhar, C. Levy, B.D. Padalia, R. Vijayaraghavan, Superconductivity at 12 K in the Y-Ni-B system. Solid State Commun. **87**, 413–416 (1993)
121. R. Nagarajan, C. Mazumdar, Z. Hossain, S.K. Dhar, K.V. Gopalakrishnan, L.C. Gupta, C. Godart, B.D. Padalia, R. Vijayaraghavan, Bulk superconductivity at an elevated temperature (T_c ~12 K) in a nickel containing alloy system Y-Ni-B-C. Phys. Rev. Lett. **72**, 274–277 (1994)
122. L.C. Gupta, Quaternary borocarbide superconductors. Phil. Mag. B **77**, 717–726 (1998)
123. H. Schmidt, H.F. Braun, in *Studies of High Temperature Superconductors*, vol. 26, ed. by A.V. Narlikar (Nova Science, Commack, New York, 1998), p. 47
124. N. Khare, A.K. Gupta, S. Khare, L.C. Gupta, R. Nagarajan, Z. Hossain, R. Vijayaraghavan, Radio frequency-SQUID effect in YNi_2B_2C due to natural grain boundary weak links. Appl. Phys. Lett. **69**, 1483–1485 (1996)
125. S. Brongersma, J. Pothuizen, E. Verweij, N. Koeman, D.G. Groot, R. Griessen, Multiple maxima in the field dependent magnetisation of superconducting Nb/Cu multilayers. J. Alloys Compounds **195**, 443–446 (1993)
126. M. Ziese, P. Esquinazi, P. Wagner, H. Adrian, S.H. Brongersma, R. Griessen, Matching and surface barrier effects of the flux-line lattice in superconducting films and multilayers. Phys. Rev. B **53**, 8658–8670 (1996)
127. M. Marezio, P.D. Dernier, A. Menth, G.W. Hull, jr., The crystal structure of $NbSe_2$ at 15 °K. J. Solid State Chem. **4**, 425–429 (1972)
128. K. Tahara, S. Lei, J. Adisoejoso, S. De Feyter, Y. Tobe, Supramolecular surface-confined architectures created by self-assembly of triangular phenylene–ethynylenemacrocycles *via* van der Waals interaction. Chem. Commun. **46**, 8507–8525 (2010)
129. L. Wang, Y. Shi, M. Liu, A. Zhang, Y.-L. Hong, R. Li, Q. Gao, M. Chen, W. Ren, H.-M. Cheng, Y. Li, X.-Q. Chen, Intercalated architecture of MA_2Z_4 family layered van der Waals materials with emerging topological, magnetic and superconducting properties. Nature Commun. **12**, 2361 (2020)
130. K. Conder, A second life of the Matthias' rules. Supercond. Sci. Technol. **29**, 080502 (2016).

131. L. Sun, R.J. Cava, High-entropy alloy superconductors: status, opportunities, and challenges. Phys. Rev. Mater. **3**, 090301 (2019)
132. J. Kitagawa, S. Hamamoto, N. Ishizu, Cutting edge of high-entropy alloy superconductors from the perspective of materials research. Metals **10**, 1078 (2020)
133. W.L. Nelson, A.T. Chemey, M. Hertz, E. Choi, D.E. Graf, S. Latturner, T.E. Albrecht-Schmitt, K. Wei, R.E. Baumbach, Superconductivity in a uranium containing high entropy alloy. Sci. Rep. **10**, 4717 (2020)
134. S. Marik, K. Motla, M. Varghese, K.P. Sajilesh, D. Singh, Y. Breard, P. Boullay, R.P. Singh, Superconductivity in a new hexagonal high-entropy alloy. Phys. Rev. Mater. **3**, 060602(R) (2019)
135. Y. Mizuguchi, Superconductivity in high-entropy-alloy telluride $AgInSnPbBiTe_5$. J. Phys. Soc. Jpn. **88**, 124708 (2019)
136. J. Wu, B. Liu, Y. Cui, Q. Zhu, G. Xiao, H. Wang, S. Wu, G. Cao, Z. Ren, Polymorphism and superconductivity in the V-Nb-Mo-Al-Ga high-entropy alloys. Sci. China Mater. **63**, 823–831 (2020)
137. E.F. Talantsev, R.C. Mataira, W.P. Crump, Classifying superconductivity in Moiré graphene superlattices. Sci. Rep. **10**, 212 (2020)
138. L. An, X. Cai, D. Pei, M. Huang, Z. Wu, Z. Zhou, J. Lin, Z. Ying, Z. Ye, X. Feng, R. Gao, C. Cacho, M. Watson, Y. Chen, N. Wang, Interaction effects and superconductivity signatures in twisted double-bilayer WSe_2. Nanoscale Horiz. **5**, 1309 (2020)
139. T. Skoskiewicz, Superconductivity in the palladium-hydrogen and palladium-nickel-hydrogen systems. Phys. Stat. Sol. A **11**, K 123–K126 (1972)
140. J.M. McMahon, M. Morales, C. Pierleoni, D.M. Ceperley, The properties of hydrogen and helium under extreme conditions. Rev. Mod. Phys. **84**, 1607–1653 (2012)
141. M. Somayazulu, M. Ahart, A.K. Mishra, Z.M. Geballe, M. Baldini, Y. Meng, V.V. Struzhkin, R.J. Hemley, Evidence for superconductivity above 260 K in lanthanum superhydride at megabar pressures. Phys. Rev. Lett. **122**, 027001 (2019)
142. Z.M. Geballe, H. Liu, A.K. Mishra, M. Ahart, M. Somayazulu, Y. Meng, M. Baldini, R.J. Hemley, Synthesis and stability of lanthanum superhydrides. Angew. Chem. Int. Ed. **57**, 688–692 (2018)
143. I. A. Kruglov, D.V. Semenok, H. Song, R. Szczęśniak, I.A. Wrona, R. Akashi, M. Mahdi Davari Esfahani, D. Duan, T. Cui, A.G. Kvashnin, A.R. Oganov, Superconductivity of LaH_{10} and LaH_{16} polyhydrides. Phys. Rev. B **101**, 024508 (2020)